Monthly Notices
of the
ROYAL ASTRONOMICAL SOCIETY

MNRAS **449,** 3927–3944 (2015) doi:10.1093/mnras/stv500

Morphological fractions of galaxies in WINGS clusters: revisiting the morphology–density paradigm

G. Fasano,[1⋆] B. M. Poggianti,[1] D. Bettoni,[1] M. D'Onofrio,[2] A. Dressler,[3] B. Vulcani,[4] A. Moretti,[1] M. Gullieuszik,[1] J. Fritz,[5,6] A. Omizzolo,[1,7] A. Cava,[8] W. J. Couch,[9] M. Ramella[10] and A. Biviano[10]

[1]*INAF, Osservatorio Astronomico di Padova, Vicolo Osservatorio 5, 35122 Padova, Italy*
[2]*Dip. di Fisica e Astronomia G. Galilei, Università di Padova, Vicolo dell'Osservatorio 2, I-35122 Padova, Italy*
[3]*The Observatories of the Carnegie Institution of Washington, Pasadena, CA 91101, USA*
[4]*Kavli Institute for the Physics and Mathematics of the Universe (WPI), Todai Institutes for Advanced Study, the University of Tokyo, Kashiwa 277-8582, Japan*
[5]*Centro de Radioastronomìa y Astrofisica, CRyA, UNAM, Campus Morelia, A.P. 3-72, C.P. 58089 Michoacàn, Mexico*
[6]*Sterrenkundig Observatorium, Universiteit Gent, Krijgslaan 281 S9, B-9000 Gent, Belgium*
[7]*Specola Vaticana, 00120 Stato Città del Vaticano, Italy*
[8]*Observatoire de Genève, Universitè de Genève, 51 Ch. des Maillettes, 1290 Versoix, Switzerland*
[9]*Center for Astrophysics, Swinburne University of Technology, Hawthorn VIC 3122, Australia*
[10]*INAF, Osservatorio Astronomico di Trieste, Via G.B. Tiepolo, 11, I-34131 Trieste, Italy*

Accepted 2015 March 3. Received 2015 March 2; in original form 2015 January 26

ABSTRACT

We present the morphology–density and morphology–radius relations (T–Σ and T–R, respectively) obtained from the WIde-field Nearby Galaxy-cluster Survey (WINGS) data base of galaxies in nearby clusters. Aiming to achieve the best statistics, we exploit the whole sample of galaxies brighter than $M_V = -19.5$ (5504 objects), stacking up the 76 clusters of the WINGS survey altogether. Using this global cluster sample, we find that the T–Σ relation holds only in the inner cluster regions ($R < 1/3\,R_{200}$), while the T–R relation keeps almost unchanged over the whole range of local density. A couple of tests and two sets of numerical simulations support the robustness of these results against the effects of the limited cluster area coverage of the WINGS imaging. The above mentioned results hold for all cluster masses (X-ray luminosity and velocity dispersion) and all galaxy stellar masses (M_*). The strength of the T–Σ relation (where present) increases with increasing M_*, while this effect is not found for the T–R relation. Noticeably, the absence/presence of subclustering determines the presence/absence of the T–Σ relation outside the inner cluster regions, leading us to the general conclusion that the link between morphology and local density is preserved just in dynamically evolved regions. We hypothesize that some mechanism of morphological broadening/redistribution operates in the intermediate/outer regions of substructured ('non-relaxed') clusters, producing a strong weakening of the T–Σ relation.

Key words: galaxies: clusters: general – galaxies: evolution – galaxies: general – galaxies: structure.

1 INTRODUCTION

The detection of significant differences in the galaxy populations between clusters and field dates back to Hubble & Humason (1931), who noted that 'the predominance of early types is a conspicuous feature of clusters in general'. 20 yr later, the prevalence in clusters of stellar Population II galaxies (early types, mainly S0s) was interpreted by Spitzer & Baade (1951) as due to galaxy collisions in the dense cluster environment. Attempts to classify clusters according to the galaxy morphological composition were subsequently made by Morgan (1961) and Oemler (1974).

Yet, the first quantitative assessment of the relation between galaxy morphology and environment was provided by Dressler (1980, hereafter D80), based on photographic plates of 55 rich galaxy clusters, obtained using the Las Campanas 2.5-m and the

⋆ E-mail: giovanni.fasano@oapd.inaf.it

Kitt Peak 4-m telescopes. Indeed, it was after this classical paper that the relation between the local projected density of galaxies in the sky (computed using the 10 nearest neighbours; Σ_{10} hereafter) and the fraction of galaxies of different morphological types (the morphology–density relation; T–Σ hereafter) began to be considered among the most important empirical evidences of extragalactic astronomy. In particular, the D80 finding that the T–Σ relation holds in both structurally regular (dynamically 'relaxed') and irregular (clumpy, 'non-relaxed') nearby clusters and its rapid extension to the group and general field environments (Bhavsar 1981; de Souza et al. 1982; Postman & Geller 1984), led the astronomical community to consider this relation a sort of universal rule in the extragalactic astronomy. Indeed, the fact that early-type galaxies (Es and S0s; ETGs hereafter) preferentially dominate dense environments, while late-type galaxies (spirals and irregulars; LTGs hereafter) are more common in low-density regions has progressively become an out-and-out paradigm with which to reckon when dealing with problems related to the evolution of galaxies, from both the phenomenological and theoretical side. For instance, Evrard, Silk & Szalay (1990) explored a model in which galaxy morphology is intrinsically related to the peak height of the initial fluctuations in a cold dark matter (CDM) universe, finding good agreement with D80 for the T–Σ relation of Es.

Besides the existence of the T–Σ relation in galaxy clusters, in D80 it is also claimed that this relation is much stronger than the relation between morphology and clustercentric distance (morphology–radius relation; T–R hereafter). However, a different viewpoint was proposed by Whitmore & Gilmore (1991), who re-examined the D80 data, finding that the strengths of the T–R and T–Σ relations are comparable. They also suggested that the physical mechanisms driving the gradients for Es are different from those operating for spirals and S0s. Whitmore & Gilmore (1993) examined again the D80 sample concluding that the T–R, normalized to a characteristic radius (R_c), is the fundamental relation driving the morphological fractions of all types, from spiral galaxies (slightly decreasing towards the centre, then going close to zero near the centre) to S0s (moderately increasing towards the centre for $R/R_c < 0.2$, then sharply falling down) and Es (from 10 per cent in the outer regions to ∼16 per cent at $R/R_c \sim 1$, then rapidly increasing up to 60–70 per cent in the inner regions). Moreover, Whitmore (1995) analysed compact and loose groups and the field, finding that the T–Σ is not present in these environments, just strongly rising near the centre of clusters.

The Whitmore & Gilmore's viewpoint about the prevalence of the T–R over the T–Σ relation in determining the morphological fractions in clusters was almost bailed out after the T–Σ relation was proved by the Morphs group (Dressler et al. 1997, hereafter D97) to hold also for intermediate-redshift clusters ($z \sim 0.5$; see also Fasano et al. 2000, in the redshift range 0.1–0.25). In this redshift range, however, the relation is found very weak or even absent for irregular clusters. Moreover, we mention that Treu et al. (2003) claimed the clustercentric distance to be the driving parameter of the ETG fraction in the inner part of the cluster Cl 0024+16 at $z \sim 0.4$.

Although structure and morphology are intrinsically different properties, thus making dangerous to compare visual T–Σ (morphology) at low z with structural T–Σ (Sérsic index) at high z (van der Wel 2008), in the subsequent decade several authors studied the T–Σ relation in different ranges of redshift and stellar mass. Most of them agreed that (i) the T–Σ is already in place, although in a less strong fashion (Postman et al. 2005), at $z \sim 0.5$, both in groups and (possibly from $z \sim 1$) in clusters (Treu et al. 2003; Smith et al. 2005; Desai et al. 2007; Wilman et al. 2009); (ii) the evolution of morphological fractions strongly depends on galaxy mass (Nuijten et al. 2005; Oesch et al. 2010; Vulcani et al. 2011); (iii) in dense environments the ETGs dominate at all redshifts and their fraction increases over time (Nuijten et al. 2005; Smith et al. 2005; Capak et al. 2007), mostly because of the growing fraction of S0s (Postman et al. 2005; Vulcani et al. 2011); (iv) the evolution of the T–Σ relation turns out to be less strong for mass limited than for magnitude limited samples (Holden et al. 2007; van der Wel et al. 2007; Tasca et al. 2009).

Besides the T–Σ dependence on redshift, some papers have also analysed the morphological fractions as a function of the global cluster properties. In particular, Desai et al. (2007) found a mild dependence of the morphological fractions on the cluster velocity dispersion, while the growth of the spiral/S0 fraction with redshift was found by Poggianti et al. (2009) to be stronger for low-mass than for high-mass clusters. A specific effect of the cluster environment on the spiral/S0 fraction is claimed by Calvi et al. (2012), based on the sharp enhancement/dearth of S0s/late types found in clusters at decreasing redshift, compared to other environments (single galaxies, binary systems, poor/rich groups).

A totally different and innovative approach to the T–Σ has been proposed with the *kinematic* morphology–density relation by Cappellari et al. (2011, Paper VII of the ATLAS^{3D} Collaboration). Rather than rely on the visual morphology, they classify galaxies according to their stellar kinematics, dividing ETGs into slow- and fast rotators (instead of Es and S0s). In this way and adopting a very local density estimator, computed just using the three nearest neighbours (the ATLAS^{3D} galaxies mainly inhabit low-density environments), they found a T–Σ cleaner than using classic morphology. They interpret this improvement is due to the fact that many fast-rotators, visually classified Es are actually face-on, misclassified S0s.

WIde-field Nearby Galaxy-cluster Survey (WINGS) is a multiwavelength photometric and spectroscopic survey of 77 galaxy clusters at $0.04 < z < 0.07$ (Fasano et al. 2006, hereafter F06). Clusters were selected in the X-ray from the *ROSAT* Brightest Cluster Sample and its extension (Ebeling et al. 1998, 2000) and the X-ray brightest Abell-type cluster sample (Ebeling et al. 1996). WINGS has obtained wide-field optical photometry (BV) for all 77 fields (WINGS-OPT; Varela et al. 2009), as well as infrared (JK) photometry (WINGS-NIR; Valentinuzzi et al. 2009), multifibre spectroscopy (WINGS-SPE; Cava et al. 2009) and U-band photometry (WINGS-U; Omizzolo et al. 2014) for a subset of the WINGS clusters. Surface photometry and morphology of WINGS galaxies have been obtained through the purposely devised, automatic tools GASPHOT (D'Onofrio et al. 2014) and MORPHOT (Fasano et al. 2012, hereafter F12), respectively. A full description of the WINGS data base is given in Moretti et al. (2014).

Exploiting the large and coherent data base provided by the WINGS project, we revisit here the T–Σ and T–R relations in galaxy clusters of the local Universe. In particular, thanks to the large galaxy sample, we are in the position of testing how these relations behave in different ranges of clustercentric distance (for T–Σ) and local density (for T–R), as well as for galaxies in different stellar mass ranges and for different global cluster properties. In Section 2 we describe the cluster and galaxy samples. In Section 3 we give detailed information about the data used to perform the analysis. The procedure used to account for and remove field galaxies is described in Section 4. Section 5 and Appendix A are devoted to characterize the issue related to the limited cluster area coverage of the WINGS imaging and to investigate the effect of such an

issue on the results we obtain for the T–Σ and T–R relations. These results are presented in Sections 6. In particular, in Sections 6.3 and 6.4 we investigate how T–Σ and T–R depend on the global cluster properties and on the galaxy stellar mass, respectively. In Section 7 we summarize our results and try to outline possible scenarios able to interpret them.

Throughout the paper we adopt a flat geometry of the Universe with the following cosmology: $H_0 = 70$ km s^{-1} Mpc^{-1}, $\Omega_{\rm M} = 0.3$ and $\Omega_\Lambda = 0.7$.

2 THE SAMPLE

2.1 The cluster sample

The galaxies used for the present analysis are located in the fields of 75 clusters belonging to the WINGS-OPT survey (see table 5 in F06). The cluster A3164 has been excluded due to the poor point spread function (PSF) quality which prevented us from obtaining a reliable morphological classification. Moreover, when performing the analysis of the T–R relation, we excluded the galaxies in the field of clusters A311, A2665 and ZwCl 1261. In fact, for these clusters we do not have a redshift coverage sufficient to allow a reliable estimation of the velocity dispersion, which is needed to compute the characteristic cluster radius R_{200} (as defined in Section 3.3) and normalize the distance of galaxies from the cluster centre.

2.2 The galaxy sample

Our starting sample of galaxies roughly coincides with that illustrated in F12. More precisely, the MORPHOT catalogue of 39 923 WINGS galaxies has been cross-matched with the catalogue of structural parameters obtained running GASPHOT on to the V-band WINGS imaging (D'Onofrio et al. 2014). This catalogue provides apparent total magnitudes and structural parameters of galaxies. The apparent magnitudes have been corrected for galactic extinction using the maps in Schlegel, Finkbeiner & Davis (1998). The galaxies for which the Sérsic index derived by GASPHOT turned out to coincide with the boundary values of the allowed search interval (0.5–8) have been excluded from the data base. In fact, in these cases we assume that a failure of the GASPHOT fitting occurred, thus preventing us from relying on the output GASPHOT parameters. For the resulting sample of 39 304 objects, putting together the data from WINGS-SPE (Cava et al. 2009) and from the literature, we gathered spectroscopic redshifts of 9361 galaxies, of which 6297 are cluster members. The absolute magnitudes of all galaxies in our sample, but the spectroscopic non-members, are computed using the average redshifts of clusters given in Cava et al. (2009) and the cosmology given in Section 1. They are K-corrected using the tables in Poggianti (1997) and according to the morphological types provided by MORPHOT (see Section 3.1).

When comparing our results with those reported in the literature, we will mainly advert to D80 and D97, which still remain the most important and cited references on this subject. After accounting for the different waveband and cosmology, the absolute V-band magnitude limits ($M_V^{\rm lim}$) given in these papers for the galaxy samples are -19.67 and -19.17, respectively. We adopt $M_V^{\rm lim} = -19.5$, which is also close to the value used for the ESO Nearby Abell Clusters Survey (ENACS) sample by Thomas & Katgert (2006, $M_V^{\rm lim} = -19.57$). In this way, we are left with the final 'reference sample' of 5504 galaxies, of which 82 per cent have measured redshift and 67 per cent are cluster members.

Throughout the paper, alternative sample partitions and selection criteria will be tested, so that the actual sample size might vary from time to time, also depending on the expected field counts relative to the particular selection. For this reason, we usually report each time in the following tables the proper sample sizes before the field removal. Finally, the same above mentioned limit of luminosity ($M_V^{\rm lim} = -19.5$) is adopted for neighbour galaxies in the computation of the local densities (Section 3.2).

3 THE DATA

All quantities we describe in the followings subsections and we use in the following analysis can be easily retrieved, through the Virtual Observatory tools, following the recommendations given in Moretti et al. (2014).

3.1 Morphology

The morphological types of galaxies are taken from the data base of WINGS galaxies described in Moretti et al. (2014). This data base has been obtained running MORPHOT (F12) on the V-band WINGS-OPT imaging of galaxies with isophotal area larger than 200 pixels at the threshold of $2.5\sigma_{\rm bkg}$ (where $\sigma_{\rm bkg}$ is the standard deviation of the background). It is worth noticing that none of the WINGS-OPT galaxies with $M_V \leq -19.5$ has been removed from the final sample because of the 200 pixels cut-off adopted by MORPHOT. This means that our absolute magnitude limited sample is safe from surface brightness incompleteness (very compact galaxies).

MORPHOT is an automatic tool purposely devised to obtain morphological type estimates of galaxies in the WINGS survey. It combines a large set of diagnostics of morphology, easily computable from the digital cut-outs of galaxies. MORPHOT produces two independent estimates of the morphological type based on (i) a semi-analytical maximum likelihood technique; (ii) a neural network machine. The final estimator has proven to be almost as effective as the visual classification. In particular, it has been shown to be able to distinguish between ellipticals and S0 galaxies with unprecedented accuracy (see fig. 11 in F12).

The MORPHOT estimator (MType in the data base) is almost coincident with the revised Hubble type defined by de Vaucouleurs et al. (1991, see table 1 in F12). For the purposes in the present paper it is convenient to split the galaxy sample in three broad morphological types: (i) ellipticals (E); (ii) lenticulars (S0); (iii) spirals (Sp). With this convention, the (few) irregular galaxies in our sample are included in the Sp class and the cD galaxies are included in the E class.

Using a sample of 176 common galaxies belonging to 18 common clusters, we have compared the broad morphological type (Es/S0s/spirals) provided by MORPHOT with the corresponding classifications given in D80. The agreement turned out to be quite good for spirals (discrepancy of 2 per cent), while for Es and S0s we found a discrepancy of $\sim$20 per cent, mainly in the sense of an excess of elliptical galaxies in the MORPHOT classifications with respect to the D80 ones. The most obvious explanation of such discrepancy is that it originates from the different material used to inspect clusters: photographic plates in the original paper of D80 and CCD imaging in the WINGS survey. For this reason, one of us (AD, indeed!) has visually (and blindly) reclassified 25 discordant objects using the WINGS observing material (CCD). With the new AD classifications the discrepancy turned out to be reduced down to a physiological amount ($\sim$6 per cent).

3.2 Local density

The projected local galaxy density relative to a given galaxy is commonly defined as the number of neighbours (N_n)of the galaxy per square megaparsec. According to the prescriptions given in D80, we compute the projected local densities using the 10 nearest neighbours of the galaxy with $M_V \leq -19.5$. At variance with D80, we use a circle (rather than a rectangle) to compute the area including the 10 nearest neighbours. That is $\Sigma_{10} = 10/A_{10}$, where $A_{10} = \pi R_{10}^2$(Mpc) and R_{10}(Mpc) is the radius (in Mpc) of the smallest circle centred on the galaxy and including the 10 nearest neighbours. Numerical simulations have shown that using the circular area produces a negligible (∼0.03) downward shift of log Σ_{10} with respect to the values computed using the rectangular area.

In order to perform the correction for field contamination, rather than our incomplete membership information, we prefer to use a statistical correction based on the field counts provided by Berta et al. (2006) using the deep ESO-*Spitzer* wide-area Imaging Survey (ESIS). In particular, we compute for each cluster the number of field galaxies per Mpc^2 (N_F) up to the apparent magnitude corresponding to $M_V^{\rm lim} = -19.5$ at the cluster redshift. Moreover, in counting the neighbours within a circle centred on a given galaxy, we statistically account for the objects possibly lost because of the proximity of the galaxy to the edges of the field of view (including the gaps between the chips). We do this dividing the counts by the ratio f_c ($\leq$1) between the area actually covered by the detector and the circular area.

Starting from the nearest neighbour ($i = 1$) and progressively including the next nearest one ($i = i + 1$), we compute each time the circular area A_i (in Mpc^2) relative to the neighbour distance and the corresponding number of neighbours: $N_{i,n} = i/f_c - N_F A_i$. When $N_{i,n}$ overcomes 10, the final area A_{10} is computed interpolating between A_i and A_{i-1}.

For 24 clusters in common with Sloan Digital Sky Survey (SDSS) Data Release 7 (DR7), we complement our positional and photometric data base with SDSS information. In particular, we use the relations in Fukugita et al. (2007) to get the V-band magnitudes of SDSS galaxies from the g' and r' ones. For this galaxy sample we are allowed to obtain complete coverages within A_{10} even for galaxies close to the frame borders, thus being able to compute the Σ_{10} values ($\Sigma_{\rm SDSS}$) without correcting for the coverage fraction ($f_c = 1$). Fig. 1 illustrates how the difference between the Σ_{10} values obtained with and without SDSS information depend on the coverage fraction. It is evident from Fig. 1 that for small values of f_c the statistical correction tends to produce an overestimation of Σ_{10}. This is likely due to the negative outward density gradient in clusters, which makes the real number of galaxies lost because of the proximity to the frame edges, lower than the number obtained correcting with f_c, i.e. assuming a uniform density inside the circles. For this reason the local densities of galaxies for which no SDSS information is available have been statistically corrected using the best-fitting relation illustrated in Fig. 1: log $\Sigma_{10}^{\rm corr} = \log \Sigma_{10} + 0.178\ (f_c - 1)$.

3.3 Clustercentric distance

We derive two different clustercentric distances (R), depending on the choice of the cluster centre. The first one (R_B) assumes the brightest cluster galaxy (BCG) as cluster centre, while the second one assumes the centre of the cluster to coincide with the maximum intensity of the X-ray emission. In any case, the clustercentric distances have to be normalized to some characteristic cluster size.

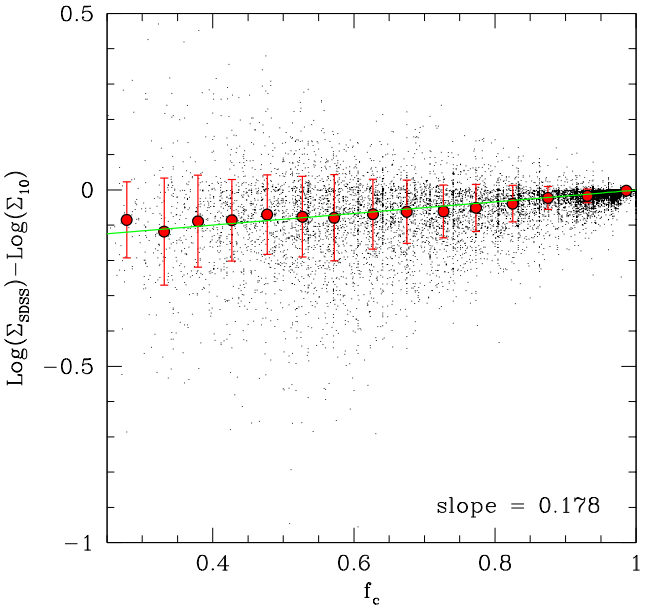

Figure 1. Difference between the Σ_{10} values obtained with and without SDSS information as a function of the coverage fraction.

One class of size estimates is based on top-hat filtered spherical overdensities. In this model, clusters are expected to be virialized within regions where the enclosed mean mass density exceeds the critical density by a factor of 200 (Peebles 1993; Peacock 1999, p. 25 and 15, respectively). We assume the radius at which this overdensity is reached, R_{200}, as the characteristic radius of the cluster. The R_{200} values for our clusters are computed from the WINGS cluster velocity dispersions (σ) given in Cava et al. (2009), using the formula (Finn et al. 2005):

$$R_{200} = 1.73 \times \frac{\sigma}{1000\,{\rm km\,s^{-1}}} \frac{1}{\sqrt{\Omega_\Lambda + \Omega_0 (1+z)^3}}\, h^{-1}\ {\rm (Mpc)}.$$

Therefore, in each cluster, the clustercentric distances of galaxies (R), to be used in the following analyses, have been obtained dividing the distance in Mpc by the proper value of R_{200}.

In Fig. 2 we illustrate, as an example, the map of the cluster Abell 1668, obtained using the photometric data from the WINGS-OPT catalogue and the morphologies provided by MORPHOT (see the figure caption for details about symbols). Similar maps of all WINGS clusters (76) are available in the online material (see the electronic version of the paper).

4 REMOVING THE FIELD GALAXIES

In order to obtain reliable T–Σ and T–R relations in nearby clusters, it is important to properly remove the contribution of field galaxies (mostly background) in each broad morphological class (E/S0/Sp). The percentages of field galaxies in each class have been estimated using the Padova–Millennium Galaxy and Group Catalogue (PM2GC; Calvi, Poggianti & Vulcani 2011; Calvi et al. 2012), consisting of a spectroscopically complete sample of galaxies at $0.03 \leq z \leq 0.11$ brighter than $M_B = -18.7$. This sample is sourced from the Millennium Galaxy Catalogue (Liske et al. 2003; Driver et al. 2005), a B-band contiguous equatorial survey, complete down to $B = 20$ and representative of the general field population in the local Universe. The advantage of using PM2GC data is that both the instrumental set-up of the imaging [Wide Field Camera (WFC) at Isaac Newton Telescope (INT)] and the tool used to estimate the

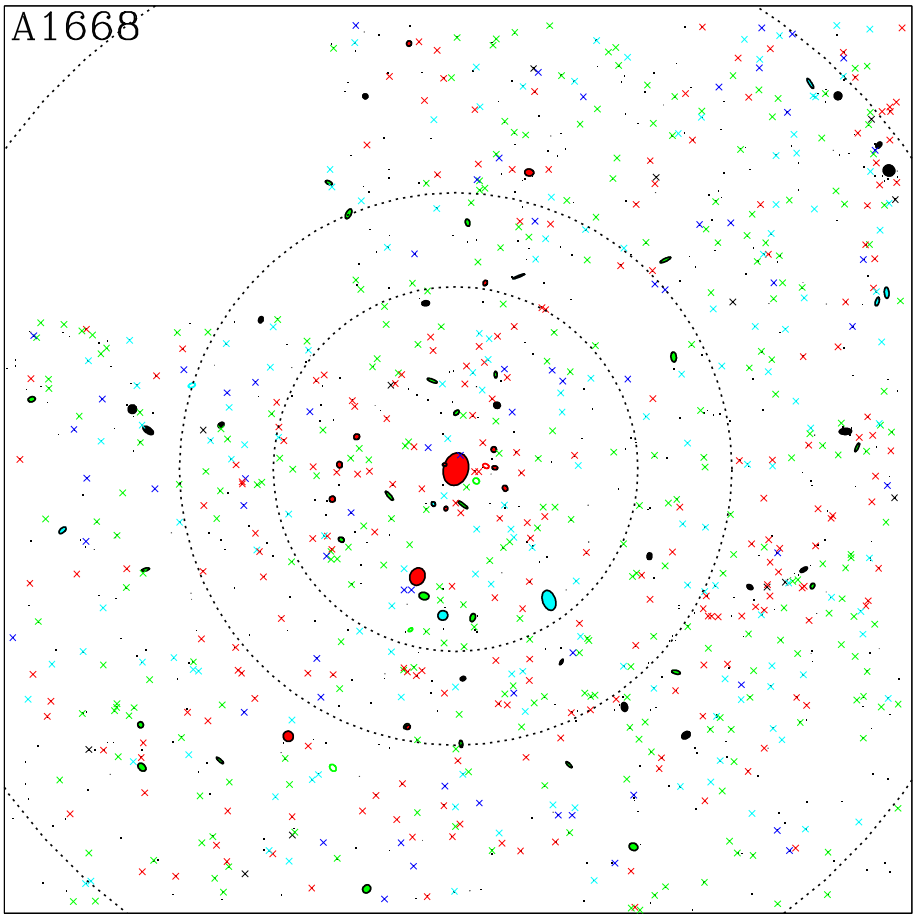

Figure 2. Map of the cluster Abell 1668, obtained using the photometric data from the WINGS-OPT catalogue and the morphologies provided by MORPHOT. The different broad morphological classifications are reported with different colours (see the online version of the paper): red for Es, green for S0s, cyan for early spirals, blue for late spirals and irregular galaxies. Small crosses refer to galaxies fainter than the limit we adopt in our analysis ($M_V > -19.5$, adopting the cluster redshift distance). Galaxies brighter than this limit are represented by ellipses, whose shapes obey the structural parameters provided by SExtractor (isophotal area, axial ratio and position angle). Spectroscopically confirmed cluster members and galaxies without spectroscopic information are indicated by full and empty ellipses, respectively, while black symbols (both ellipses and crosses) identify galaxies which, according to Cava et al. (2009), are considered spectroscopic non-members. Finally, dashed circles correspond to different distances from the BCG: 0.33, 0.5 and 1 (in R_{200} units).

morphological types (MORPHOT) are the same for both PM2GC and WINGS galaxies. This guarantees a full morphological consistency between the two samples.

Fig. 3 reports the morphological fractions of the PM2GC galaxy sample in different bins of apparent magnitude. Even if the expected increase of the E fraction and decrease of the Sp fractions are clearly detectable, Fig. 3 shows that the percentages E/S0/Sp depend weakly on the apparent magnitude. In our analysis we assume E/S0/Sp = 19.3(±3.1) per cent/21.7(±2.7) per cent/59(±5.3) per cent. These values correspond to the morphological fractions of PM2GC galaxies with $V \leq 17.77$, this limit including 95 per cent of the WINGS galaxies in our reference sample (see below).

In Fig. 4 the global field counts in the V band from the PM2GC galaxy sample are compared with the counts given by Berta et al. (2006) in the same waveband and in the magnitude range of interest for us. The slight systematic excess of the PM2GC counts for bright galaxies with respect to the counts by Berta et al. (2006) is likely due to the presence in the PM2GC field of many galaxy groups, which, because of the criteria adopted in the choice of the field, are probably lacking in the ESIS data base used by Berta et al. (2006). On the other hand, the sharp decline of the PM2GC counts towards faint galaxies clearly reveals the incompleteness of the PM2GC galaxy sample for which a morphological classification has been possible through MORPHOT (isophotal area larger than 200 pixels at the threshold of $2.5\sigma_{\rm bkg}$). Nevertheless, it is noticeable that the two counts curves assume roughly the same value (1.51, i.e. ∼32 galaxies deg^{-2}) at $V \leq 17.77$, which is the value chosen above to compute our morphological fractions. All things considered, the statistical counts of field galaxies suggest us to remove in our analyses 32 galaxies deg^{-2}, in particular: six Es (19.3 per cent), seven S0s (21.7 per cent) and 19 spirals (59 per cent).

According to Section 2.2, in our galaxy sample the global spectroscopic coverage and cluster membership, up to the adopted limit of absolute V-band magnitude (−19.5), are 82 and 67 per cent, respectively. These rather high percentages allowed us to deal with the problem of field galaxies using a strategy complementing the statistical field counts with the membership information. In particular, we first removed from the sample those galaxies which, according to the redshift information and the membership criteria described in Cava et al. (2009), are not cluster members. Then, if the number of galaxies removed from each broad morphological class (Es/S0s/Sp) turned out to be lower than the expected field counts relative to that class, we further subtracted from the residual the quantity needed to reach the field counts expected from Berta et al. (2006). In this

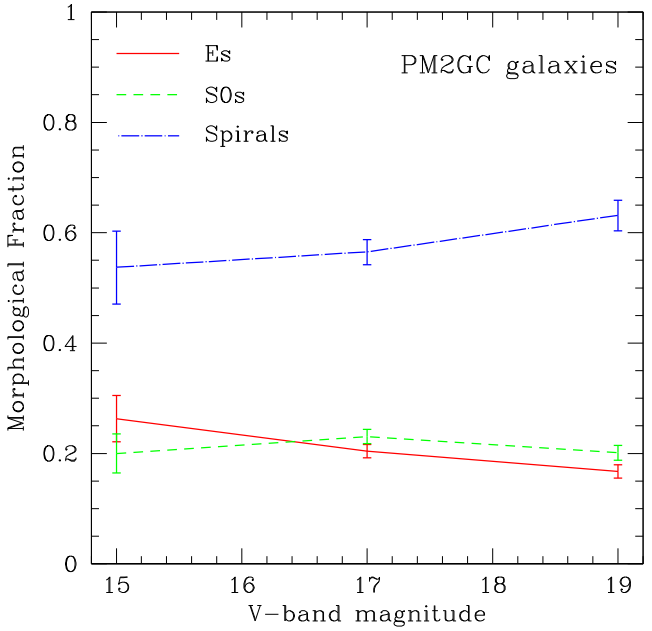

Figure 3. Morphological fractions of PM2GC galaxies as a function of the apparent *V*-band magnitude. Error bars report the Poissonian uncertainties.

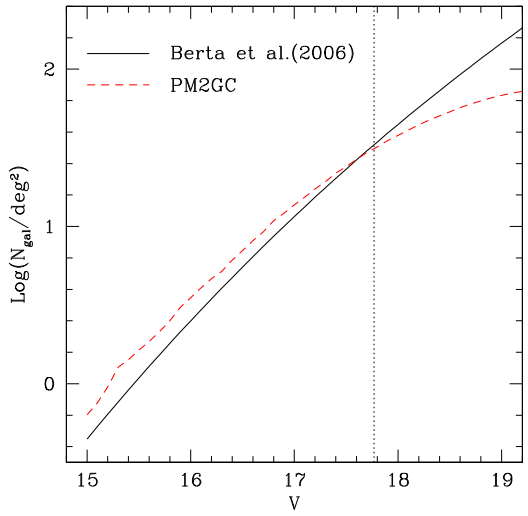

Figure 4. Counts of field galaxies from Berta et al. (2006) and from PM2GC. The vertical dotted line corresponds to the apparent magnitude at which we have computed the morphological fractions ($V = 17.77$).

way, it might happen that the actual number of removed galaxies exceeds the number expected from the field counts. In any case, we have verified that the differences between the T–Σ relations obtained using our mixed strategy and a 'pure' statistical approach are practically negligible.

5 THE CLUSTER AREA COVERAGE ISSUE

Having at our disposal a large galaxy sample in a well defined, complete cluster sample, our strength lies in the opportunity to take advantage of a good statistics. For this reason, in the present analysis we mostly use galaxies in the whole cluster sample. At times, however, in order to perform some particular analysis, we use galaxies belonging to a subsample of clusters (selected, for instance, on the basis of X-ray emission, velocity dispersion or

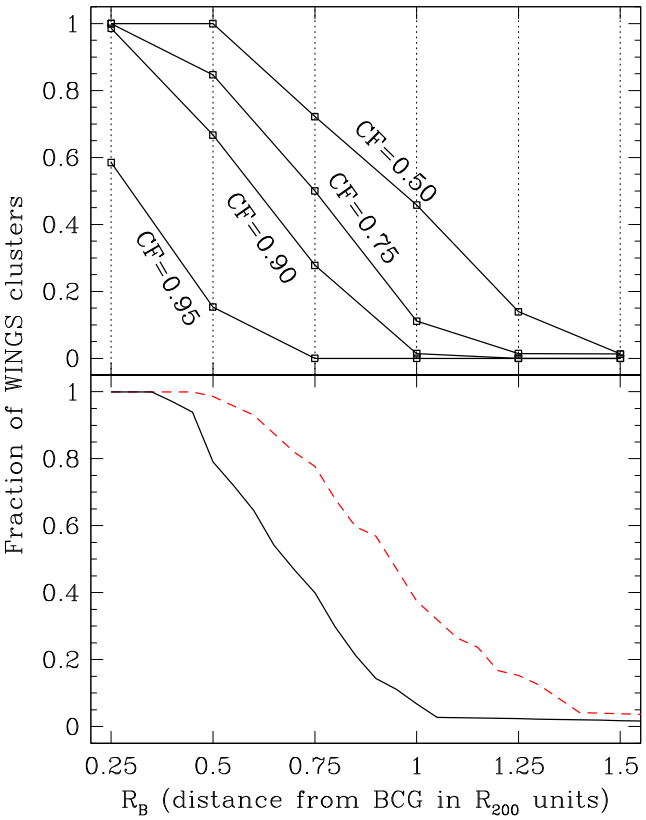

Figure 5. Upper panel: the fraction of WINGS clusters with circular coverage fraction greater than some given value (0.50, 0.75, 0.90 and 0.95) as a function of the radius (in units of R/R_{200}) of the circular area centred on the BCG. Bottom panel: the solid line reports the fraction of WINGS clusters whose equivalent radius (see text) exceeds the value of R_B reported in the abscissa. The dashed line (red in the electronic version) illustrates the fraction of WINGS clusters for which the largest clustercentric galaxy distance (R_B) exceeds the value given in the abscissa.

subclustering), or galaxies obeying some constraint (for instance on the stellar mass).

On the other hand, our weakness lies in the limited and not always regular cluster area covered by the WINGS images. The upper panel of Fig. 5 shows that, for $R_B = 0.5$, 0.75 and 1.0, the WINGS images cover more than 90 per cent of the circular (BCG centred) area in just ∼66, 28 and 2 per cent of the clusters, respectively, while a coverage fraction (CF hereafter) of 0.75 at the same radii is reached in ∼85, 50 and 11 per cent of the clusters. Similar CFs are found if we assume the cluster centres to coincide with the maximum intensity of the X-ray emission. An alternative way to illustrate the coverage problem is provided by the bottom panel of Fig. 5. In this panel the solid line reports the fraction of WINGS clusters whose equivalent radius $R_{\rm eq} = \sqrt{A_{200}/\pi}$ (A_{200} being the area covered by the WINGS images in units of R^2_{200}) exceeds the value of R_B reported in the abscissa, while the dashed line (red in the electronic version) reports the fraction of WINGS clusters for which the galaxy with the largest clustercentric distance has a R_B exceeding the value given in the abscissa.

Even if one of the goals of the present paper is the analysis of the morphological fractions as a function of the clustercentric distance (T–R), from previous studies we know that the spiral fraction inside a given (BGC or X-ray centred) cluster area is an increasing function of the radius. Thus, the limited cluster area coverage of the WINGS images in comparison with other analyses (e.g. D80; Goto et al.

2003; Thomas & Katgert 2006) is expected to result in a reduced global fraction of spirals.

Besides this obvious effect, additional biases due to the limited cluster area coverage of our data could affect the T–R and T–Σ relations we present here.

Concerning the first relation (T–R), there is no reason to believe that any galaxy included in our sample, with clustercentric distance (R) not completely covered by our imaging, should be drawn from a morphological distribution different from the average distribution at that R. Therefore, the T–R should be unaffected by both the limited cluster area coverage of our images, and their irregular shape (for INT imaging, in particular). For the T–R, the above issues should just translate into a limited extension of the relation and a relatively large Poissonian uncertainty of its outer part.

Trying to quantify the possible biases affecting the T–Σ relation because of the limited cluster area coverage of our imaging, in Appendix A we present three different tests. The first two tests investigate the effects on T–Σ of two different issues: the irregular shape of WINGS images and their limited coverage of the cluster area. The third test, performed through quite simple numerical simulations, is again aimed at investigating the effect of the limited cluster coverage on the T–Σ in different ranges of clustercentric distance. Moreover, since the simulations require some hypothesis about the driving parameter (Σ or R) of the morphological fractions, they could also provide useful indication with regards to such parameter (see Section A3 in Appendix A).

6 RESULTS: THE T–Σ AND T–R RELATIONS IN WINGS CLUSTERS

In Fig. 5 we have shown that, due to the limited field of view of the cameras used in the WINGS optical survey, the cluster area coverage of our cluster images turns out to be relatively small. As expected, this makes the global morphological content of our galaxy sample quite different from that reported in previous analyses which made use of much larger field of view imaging. In particular, we find E/S0/Sp $\sim$ 33/44/23 per cent (see also Poggianti et al. 2009; Vulcani et al. 2011, with a slightly different sample selection) to be compared with the morphological fractions given by D80 ($\sim$18/41/41 per cent) and Thomas & Katgert (2006, $\sim$19/47/34 per cent). It is worth stressing that, supported by the comparison between the MORPHOT and D80 morphological classifications (see Section 3.1), we entirely attribute to the limited cluster area coverage of the WINGS imaging the above discrepancy of global morphological fractions.

Let us now indicate with $F_{\rm fE}/F_{\rm fS0}/F_{\rm fSp} = 0.193/0.217/0.59$ the morphological fractions we have previously found for field galaxies, and with $N_{\rm tot}$ and $N_{\rm f}$ the total number of galaxies and of field galaxies relative to the particular selection (of clusters and/or galaxies and/or range of R or Σ_{10}) we are testing in the analysis of the T–Σ and T–R relations. For each bin (i) of log Σ_{10} or R_B and for each broad morphological type (T = E/S0/Sp), we compute the morphological fractions as

$$F_{\rm T}^i = \frac{N_{\rm T}^i - F_{\rm fT} N_{\rm f}^i}{N^i - N_{\rm f}^i}. \quad (1)$$

In these expressions, the symbols N and F indicate galaxy numbers and fractions, respectively. In particular, N^i and $N_{\rm T}^i$ are the total number of galaxies and the number of galaxies with broad morphological type T in the ith bin, while we indicate with $N_{\rm f}^i$ the product $N^i \times F_{\rm f}$ and with $F_{\rm f}$ the fraction $N_{\rm f}/N_{\rm tot}$. In the above formulation of $F_{\rm T}^i$ we assume that the number of field galaxies per deg^2 and the global morphological field ratios $F_{\rm fT}$ do not depend on the local density. In the following figures we just plot the bins where the number of cluster galaxies ($N^i - N_{\rm f}^i$) is greater than 10.

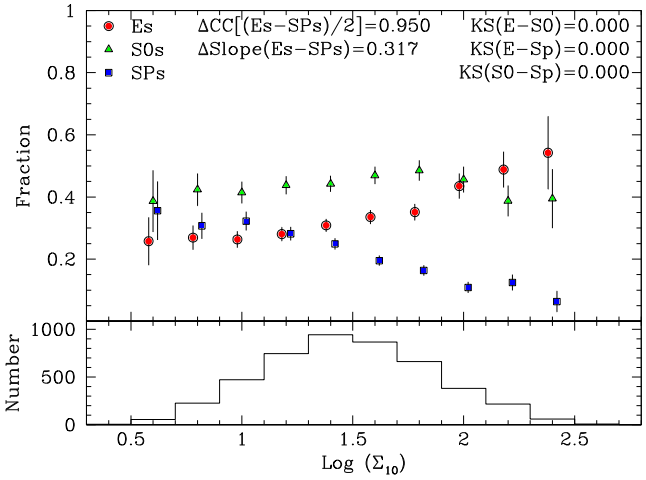

Figure 6. T–Σ (upper panel) and histogram of local density (lower panel) for the whole 'reference sample' of 5504 WINGS galaxies with $M_V \leq -19.5$. Full dots, triangles and squares (red, green and blue in the electronic version of the paper) refer to Es, S0s and spirals, respectively. The error bars correspond to Poissonian uncertainties. Details about the coefficients reported in the upper panel (KS, ΔCC and ΔSlope) are given in the text.

6.1 T–Σ relation

Fig. 6 illustrates the T–Σ relation for the whole reference sample of 5504 WINGS galaxies (see also Table 1), adopting a bin size of 0.2 in log Σ_{10}. In the upper panel of the figure and in the following T–Σ (and T–R) plots, we report a few coefficients, through which we try to quantify the differences among the fraction–log Σ_{10} (fraction–R_B for the T–R) relations relative to Es, S0s and spirals. In particular, for each pair of broad morphological types, we report the two-sample Kolmogorov–Smirnov probability (2S-KS hereafter) that the two distributions of log Σ_{10} are drawn from the same parent population. Moreover, we compare the weighted T–Σ of Es and spirals, reporting the coefficients ΔCC and ΔSlope. They give, respectively, the halved difference of correlation coefficients and the slope difference between the T–Σ of Es and spirals assuming a linear fit. These values, together with their expected rms uncertainties, are also reported in Table 1.

Fig. 6 clearly shows that for the WINGS cluster galaxies we recover the classical T–Σ relation: at increasing local density, the fractions of Es and spirals increase and decrease, respectively. The correlations are very strong in both cases, as indicated by the coefficients ΔCC and ΔSlope, while the KS(E–Sp) probability indicates that Es and spirals are quite distinct from each other. It is also worth noticing that the fraction of S0s seem not to depend at all on the local density, as found also by D97. In addition, the KS analysis suggests that the S0s constitute a population well distinct from both Es and spirals. The first row of Table 1 (columns 2, 3 and 4) reports the values of the coefficients, together with their rms uncertainties.

Let us now check out whether and how the T–Σ relation depends on the position of the galaxy inside the cluster, in particular on the clustercentric distance relative to the BCG (R_B). Fig. 7 illustrates the T–Σ in two different ranges of R_B. The left-hand panel of the figure refers to the central region of the clusters ($R_B < 0.5$), while the right-hand panel refers to the R_B interval (0.5–1). It stands out that, while in the central part of the cluster the T–Σ is quite strong, when

Table 1. Coefficients ΔCC and ΔSlope for T–Σ and T–R in different intervals of R_B and log Σ_{10}, respectively. The table also reports the 2S-KS probabilities that the log Σ_{10} or R_B distributions of elliptical and spiral galaxies are drawn from the same parent population for the T–Σ and T–R relations, respectively. The number of galaxies used in each case is reported below the R_B or log Σ_{10} intervals, while the expected rms uncertainties of the coefficients ΔCC and ΔSlope are reported below the relative values.

	T–Σ				T–R		
R_B	ΔCC	ΔSlope	KS(E–Sp)	log Σ_{10}	ΔCC	ΔSlope	KS(E–Sp)
All	0.950	0.317	0.000	0–3	0.942	0.619	0.000
(5504)	(0.024)	(0.025)		(5187)	(0.026)	(0.053)	
0–0.5	0.878	0.282	0.000	0–1.45	0.869	0.478	0.000
(3813)	(0.054)	(0.041)		(2567)	(0.055)	(0.070)	
0.5–1	0.215	0.101	0.079	1.45–3	0.878	0.602	0.000
(1321)	(0.195)	(0.083)		(2620)	(0.062)	(0.105)	
0–0.33	0.910	0.342	0.000	0–1.2	0.762	0.375	0.001
(2538)	(0.047)	(0.048)		(1331)	(0.094)	(0.080)	
0.33–0.66	0.132	0.018	0.280	1.2–1.8	0.953	0.578	0.000
(2026)	(0.195)	(0.042)		(2828)	(0.025)	(0.059)	
0.66–1	0.145	0.113	0.120	1.8–3	0.709	0.522	0.000
(570)	(0.228)	(0.134)		(1028)	(0.171)	(0.181)	
0.33–1	0.332	0.075	0.089				
(2596)	(0.184)	(0.041)					

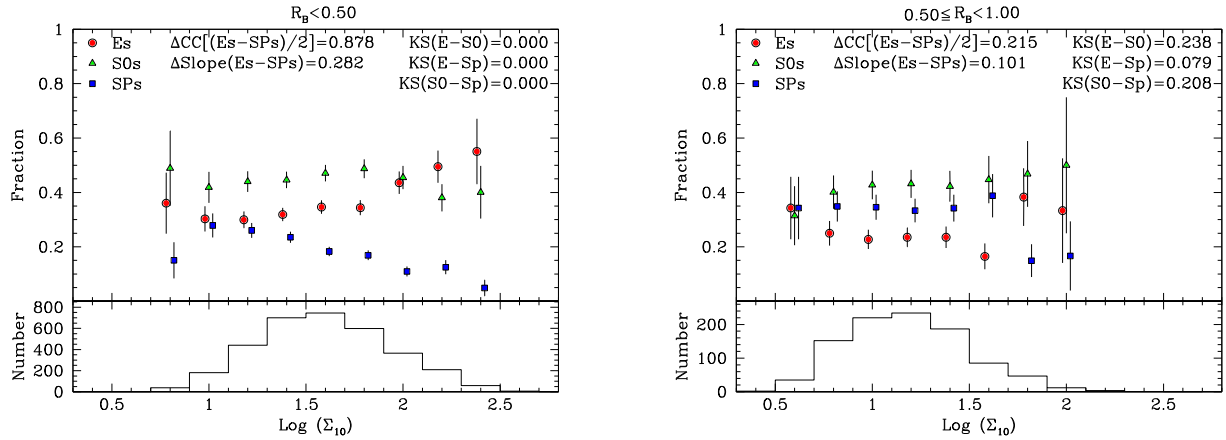

Figure 7. T–Σ for WINGS galaxies with $R_B < 0.5$ (in units of R_{200}, left-hand panel) and $0.5 \leq R_B < 1$ (right-hand panel). The meaning of the symbols is as in Fig. 6.

moving outside it seems to become very weak or even absent. This is formally confirmed by the ΔCC and ΔSlope values, as well as by the 2S-KS probabilities obtained in the two R_B intervals. These values are reported in Table 1 (rows 2 and 3; columns 2, 3 and 4).

Table 1 also reports, in rows 4, 5 and 6 (columns 2, 3 and 4), the results we obtain splitting the R_B interval (0–1) into three parts, while in the row 7 we report the data relative to the R_B interval (0.33–1), which we refer to in Fig. 12. Table 1 clearly shows that the region where the T–Σ actually operates is the very inner cluster region ($R_B < 1/3$). The high significance found for the T–Σ for the whole galaxy sample (see Fig. 6) is just due to the fact that the inner regions are the most densely populated in the clusters.

6.2 T–R relation

In the analysis of the T–R relation we assume again the cluster centre to coincide with the position of the BCG ($R \equiv R_B$), while in this case we adopt a bin size of 0.15 for R_B. We note, however, that both the previous and the following results remain practically unchanged if we adopt a different bin sizes and/or assume the cluster centre to coincide with the maximum intensity of the X-ray emission.

Figs 8 and 9 are similar to Figs 6 and 7, respectively, but refer to the T–R relation for the global sample of WINGS galaxies (Fig. 8) and for galaxies in two different ranges of the local density (Fig. 9). Columns 6, 7 and 8 of Table 1 report the values of the coefficients in these cases, as well as the values obtained splitting the log Σ_{10} interval (0–3) into three parts.

This table and the two above mentioned figures show that, at variance with the T–Σ relation, where the morphological correlations turn out to be significant just in the inner regions of clusters, the T–R relation turns out to be always significant in the cluster environment (at least out to $R \sim R_{200}$), irrespectively of the local density regime. This is highly suggestive that the T–R relation is more robust than the T–Σ one, and that the clustercentric distance is actually the driving parameter of the morphological fractions in clusters. The above conclusions seem to overturn the widespread paradigm of the morphology–density relation, making the old, alternative point of view by Whitmore & Gilmore (1991, 1993, see also Whitmore 1995) to come up again. In Section 7 we briefly discuss this point,

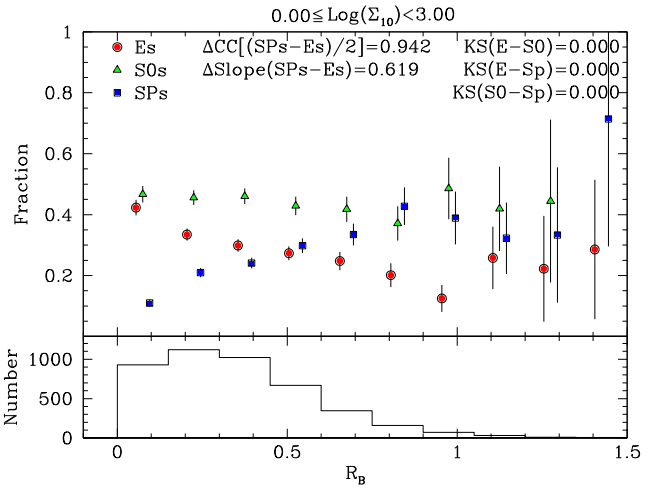

Figure 8. *T–R* (upper panel) and histogram of R_B (lower panel) for the whole sample of 5187 WINGS galaxies with $M_V \leq -19.5$ for which the value of R_B in units of R_{200} is available. The meaning of the symbols is as in Fig. 6.

trying to interpret the strong outwards weakening of T–Σ as due to some mechanism of morphological broadening/reshuffling, which could operate in the intermediate/outer regions of nearby clusters. In the meantime, it is worth mentioning that the robustness of our results seems to be supported by the tests and simulations presented in Appendix A. We are aware that they cannot fully remedy the lack of data at large clustercentric distances. Still, waiting for the conclusion of our program for very wide-field ($1^\circ \times 1^\circ$) imaging and spectroscopy of a representative subsample of the WINGS clusters,[1] we believe the results we present here should be a good approximation of those we will obtain with a more complete galaxy sample.

6.3 T–Σ and T–R for different global cluster properties

We now seek for possible dependencies of the T–Σ and T–R relations on global cluster properties. In particular, we investigate the dependencies on the X-ray luminosity ($\log L_X$) and on the velocity dispersion of galaxies in the clusters ($\log \sigma$), both quantities being somehow linked to the total cluster mass. Moreover, we analyse how the presence of substructures in the clusters influences the strength of the T–Σ and T–R relations.

6.3.1 Cluster mass

Cluster velocity dispersions were computed combining WINGS and literature redshifts. For all but one cluster, they are based on more than 20 spectroscopic members, with an average of 92 spectroscopic members per cluster (Cava et al. 2009). The X-ray luminosities (0.1–2.4 keV) from Ebeling et al. (1996, 1998, 2000) have been converted to the cosmology used in this paper.

The WINGS clusters cover a wide range of σ, typically between 500 and 1100 km s^{-1}, and L_X, typically 0.2–5 $\times$ 10^{44} erg s^{-1}.

Tables 2 and 3 are similar to Table 1 (first three rows), but they split the WINGS cluster sample in two different intervals of $\log \sigma$ and $\log L_X$, respectively. The splitting values are chosen trying to balance (as much as possible) both the width and the number of galaxies of the intervals themselves.

In spite of the expected (sometimes large) uncertainties of the coefficients ΔCC and ΔSlope, Tables 2 and 3 suggest that the results we found for the global WINGS cluster sample do not depend either on the velocity dispersion, or on the X-ray luminosity of clusters. In fact, in both cases, the galaxy subsamples obtained splitting the global WINGS cluster sample, again show the tendency of the T–Σ relation to hold just in the inner cluster regions, while the strength of the T–R relation does not seem to depend on the local density regime.

To include figures similar to previous ones for all 24 cases reported in Tables 2 and 3 would be a worthless space waste. Thus we decided to show, in Figs 10 and 11, just some examples illustrating the validity of the above conclusions (see the figure captions for more details).

6.3.2 Subclustering

The T–Σ relation has been found by D80 to hold for both regular ('relaxed') and irregular ('non-relaxed') clusters of the local Universe and this finding has given support to the idea that it is a sort of general rule in the realm of galaxies. Indeed, since, by definition, the T–Σ relation concerns the local environment, assuming such a relation to have a general validity implies it should be found everywhere, no matter what is the global structure of the cluster. On the contrary, the lack of T–Σ relation in irregular (clumpy) clusters would suggest that either it is just a by-product of the T–R relation (assuming it ever holds in such kind of clusters), or that in the cluster substructures (infalling groups?) the morphological segregation and processing still is on-going or to come, as suggested by D97 for intermediate-redshift clusters (a rather unlikely possibility for nearby clusters, indeed). Therefore, it is of some interest to test, in our large sample of nearby clusters, the effects of subclustering on the T–Σ and T–R relations. To this aim, following the classification given by the catalogue of substructures in WINGS clusters (Ramella et al. 2007, see table A1 therein), we have divided our cluster sample in three subsamples: (i) the sample *M* includes the 15 WINGS clusters for which just the main structure (M) was detected by the DEDICA algorithm (Pisani 1993, 1996); (ii) the sample *S1+* includes the 40 clusters for which DEDICA found at least one substructure (S) at the same redshift of the main structure; (iii) the sample *nd* (not detected) contains the 22 WINGS clusters whose irregular and very clumpy structure prevented DEDICA from detecting any significant structure inside them. For these cluster samples, Fig. 12 reports the coefficients ΔSlope (upper panels) and ΔCC (lower panels) of the T–Σ (left-hand panels) and T–R (right-hand panels) relations, in two ranges of R_B and $\log \Sigma_{10}$, respectively. The dashed and dotted lines (red and blue in the electronic version) correspond to the values found for the whole sample of WINGS clusters in the different cases.

Some interesting things come to light from Fig. 12: (a) in the inner part of clusters ($R_B < 0.33$) and in the regions of high local density ($\log \Sigma_{10} > 1.45$), the T–Σ and T–R relations (respectively) turn out to be quite strong in all three subsamples (full dots in the figure; red in the electronic version). In particular, in each case the strength of the relations is similar to that of the corresponding one relative to the whole cluster sample, no matter which is the subclustering level (dashed lines; see also Table 1); (b) for $R_B > 0.33$, the relation T–Σ turns out to be as strong as in the inner part of clusters just

[1] We are presently gathering *V*-, *B*- and u'-band OmegaCam at VLT Survey Telescope (VST) imaging and AAOmega+2dF at Anglo-Australian Telescope (AAT) spectroscopy for 54 clusters of the WINGS original sample.

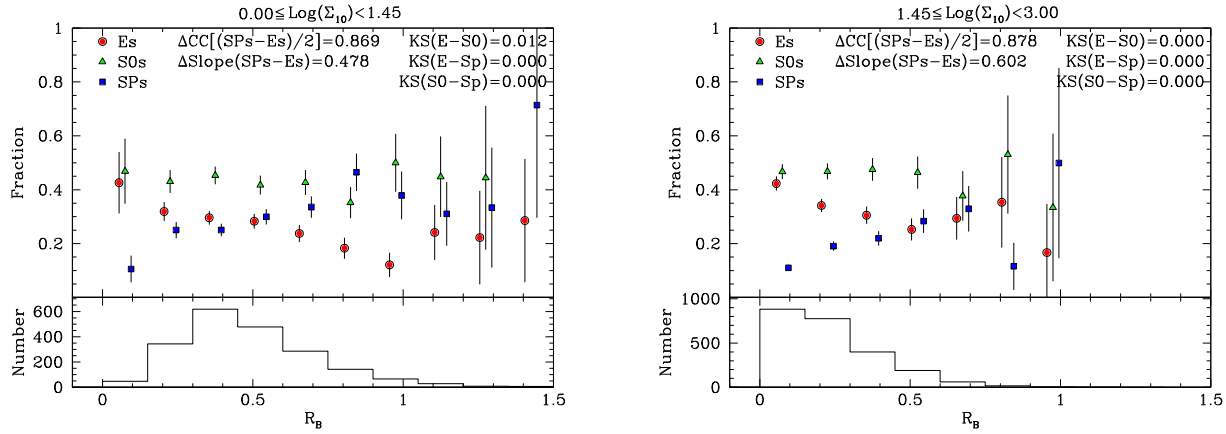

Figure 9. *T*–*R* for WINGS galaxies with log $\Sigma_{10} < 1.45$ (median value of the Σ_{10} distribution; left-hand panel) and $1.45 \leq \log \Sigma_{10} < 3$ (right-hand panel). The meaning of the symbols is as in Fig. 6.

Table 2. Similar to Table 1, but for two different intervals of log σ.

		T–Σ				*T*–*R*		
log σ	R_B	ΔCC	ΔSlope	KS(E–Sp)	log Σ_{10}	ΔCC	ΔSlope	KS(E–Sp)
	All	0.927	0.368	0.000	0–3	0.937	0.593	0.000
	(2129)	(0.034)	(0.040)		(2112)	(0.029)	(0.054)	
<2.85	0–0.5	0.757	0.277	0.000	0–1.45	0.871	0.527	0.000
	(1222)	(0.113)	(0.064)		(1334)	(0.054)	(0.074)	
	0.5–1	0.289	0.100	0.425	1.45–3	0.854	0.620	0.000
	(816)	(0.226)	(0.077)		(778)	(0.096)	(0.153)	
	All	0.862	0.298	0.000	0–3	0.936	0.690	0.000
	(3106)	(0.066)	(0.042)		(3075)	(0.031)	(0.077)	
≥2.85	0–0.5	0.812	0.280	0.000	0–1.45	0.746	0.430	0.000
	(2591)	(0.085)	(0.054)		(1233)	(0.113)	(0.117)	
	0.5–1	0.083	0.075	0.083	1.45–3	0.961	0.727	0.000
	(505)	(0.192)	(0.122)		(1842)	(0.022)	(0.073)	

Table 3. Similar to Table 1, but for two different intervals of log (L_X).

		T–Σ				*T*–*R*		
log (L_X)	R_B	ΔCC	ΔSlope	KS(E–Sp)	log Σ_{10}	ΔCC	ΔSlope	KS(E–Sp)
	All	0.883	0.315	0.000	0–3	0.887	0.635	0.000
	(2363)	(0.054)	(0.039)		(2192)	(0.049)	(0.077)	
<44.15	0–0.5	0.710	0.256	0.000	0–1.45	0.852	0.550	0.000
	(1524)	(0.117)	(0.068)		(1223)	(0.062)	(0.090)	
	0.5–1	0.276	0.136	0.236	1.45–3	0.885	0.949	0.000
	(628)	(0.223)	(0.108)		(969)	(0.075)	(0.176)	
	All	0.943	0.297	0.000	0–3	0.936	0.615	0.000
	(3041)	(0.025)	(0.027)		(2895)	(0.031)	(0.067)	
≥44.15	0–0.5	0.878	0.258	0.000	0–1.45	0.740	0.432	0.000
	(2228)	(0.054)	(0.038)		(1277)	(0.116)	(0.107)	
	0.5–1	0.060	0.042	0.122	1.45–3	0.944	0.562	0.000
	(653)	(0.225)	(0.120)		(1618)	(0.033)	(0.070)	

for the subsample *M*, which presumably contains the most regular ('relaxed') clusters, while for the other two subsamples (*S1*+ and *nd*) the lack of relation is confirmed at a significance level even greater than in the case of the whole cluster sample; (c) in the lower bin of local density (log $\Sigma_{10} < 1.45$), the *T*–*R* relation remains strong for both the *M* and *S1*+ subsamples, becoming weaker just for the subsample *nd*.

In Fig. 13 the *T*–Σ and *T*–*R* relations (upper and bottom panels, respectively) for the regular (left-hand panels; sample *M*) and very irregular (right-hand panels; sample *nd*) clusters are illustrated for some particularly interesting cases. The upper panels clearly show that (i) for regular clusters the *T*–Σ relation holds outside the very inner regions too (at variance with our finding relative to the global cluster sample); (ii) in the inner cluster regions the *T*–Σ relation holds even for very irregular clusters (not a trivial thing, indeed). The bottom panels show that the *T*–*R* relation, in the whole range of Σ_{10}, holds for both regular and very irregular clusters.

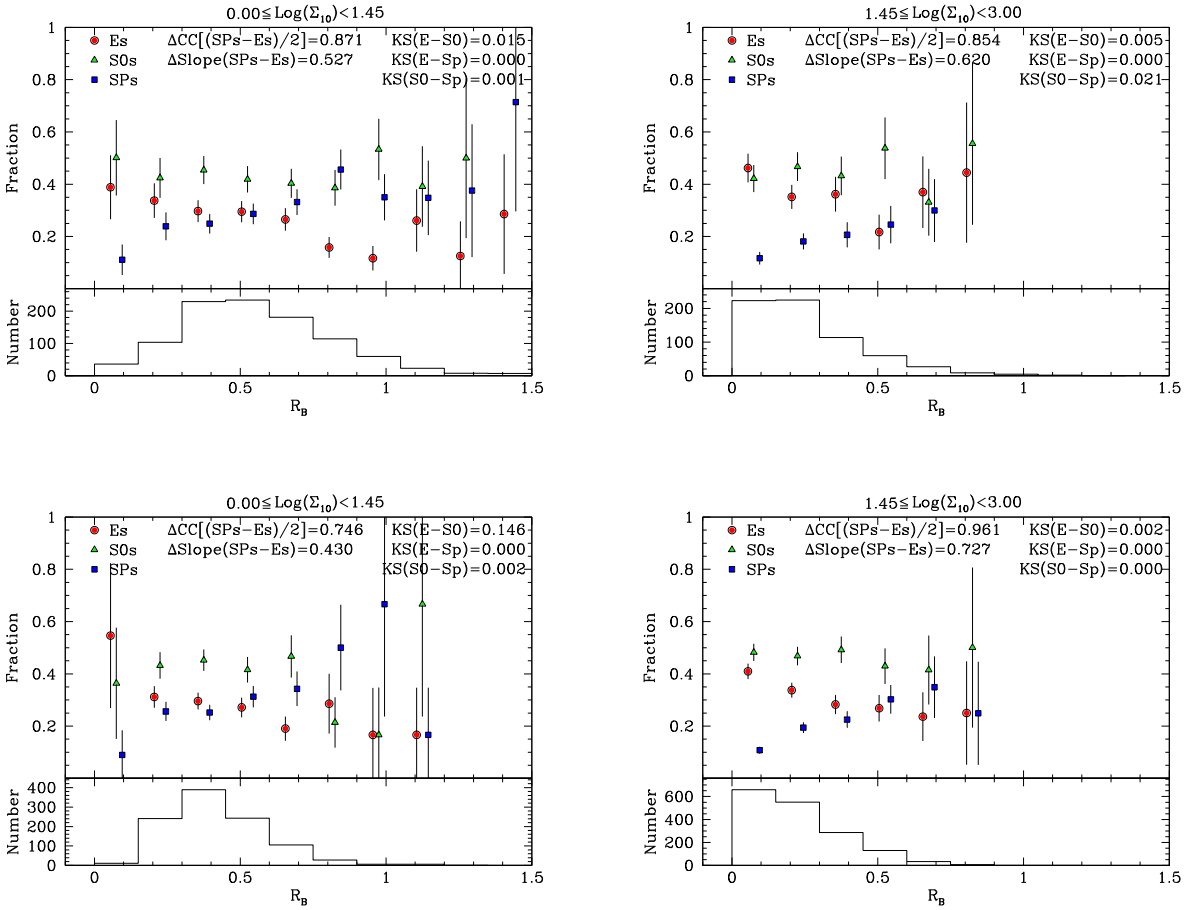

Figure 10. *T–R* relation for clusters with log $\sigma < 2.85$ (upper panels) and log $\sigma \geq 2.85$ (bottom panels) in different ranges of local density: log $\Sigma_{10} < 1.45$ (left-hand panels) and $1.45 \leq \log \Sigma_{10} < 3$ (right-hand panels). Even at a first glance, in both intervals of log σ the *T–R* relation appears to hold over the whole range of local density. The meaning of the symbols is as in Fig. 6.

6.4 *T*−Σ and *T*−*R* for different stellar masses

Peng et al. (2010), using the surveys SDSS and zCOSMOS (Lilly et al. 2007; Scoville et al. 2007), have analysed the fraction of quenched galaxies in the general field as a function of both the stellar mass and the environment, over the cosmic time. More closely in connection with our investigation, the dependence of global morphological fractions on galaxy stellar mass in clusters at different redshifts has been analysed by Vulcani et al. (2011). However, the possible dependence of the *T*–Σ and *T–R* relations on M_* has not been investigated so far, apart from some particular aspects of the problem analysed by Bamford et al. (2009). In this analysis the fraction of early-type galaxies are found to increase with the local density in each bin of stellar mass, the slope of the fraction–log Σ_{10} relation being almost the same in all bins. However, this study is based on the morphological classifications provided by the Galaxy Zoo project (Lintott et al. 2011), being thus limited by the lack of distinction between ellipticals and S0 galaxies.

Stellar masses of WINGS galaxies (Fritz et al. 2011) have been determined by fitting the optical spectrum (in the range ∼3600–∼7000 Å) with the spectrophotometric model fully described in Fritz et al. (2007). In this model, all the main spectrophotometric features are reproduced by summing the theoretical spectra of simple stellar population (SSP) of 13 different ages (from 3×10^6 to $\sim 14 \times 10^9$ yr) and assuming a Salpeter initial mass function (IMF). Dust extinction is allowed to vary as a function of SSP age and the metallicity can vary among three values: $Z = 0.004$, 0.02 and 0.05. These mass estimates were then corrected for colour gradients within each galaxy (i.e. for the difference in colour within the fibre and over a 10-kpc diameter) and were converted to the Kroupa (2001) IMF. Fritz et al. (2011) provide mass estimates for ∼5300 WINGS galaxies, 1540 of them belonging to the galaxy sample we use in this paper. In Vulcani et al. (2011) it is shown that these mass estimates are in fairly good agreement with those derived using the rest-frame $(B - V)$ colours and the recipe given in Bell & de Jong (2001).

Table 4 is similar to previous Tables 2 and 3, but it splits the WINGS galaxies in two intervals of log (M_*). In this case the splitting value roughly coincides with the median of the log (M_*) distribution. Provided that the *T*–Σ for this reduced galaxy sample proves again itself to be weak or absent outside the inner cluster regions, from Table 4 it turns out that the strength of the *T*–Σ relation is greater in the high-mass than in the low-mass bin. We decided to further explore this point dividing the stellar mass interval in four relatively narrow bins of size 0.5, starting from log $(M_*) = 10$.[2]

[2] The spectroscopic magnitude limit of the WINGS survey is $V = 20$, corresponding to a mass limit of log $(M_*) = 9.8$. Vulcani et al. (2011) actually report that the completeness of mass limited samples in WINGS is reached for log $(M_*) = 10.5$. Thus, the lowest mass bin in Fig. 14 could still suffer from some bias.

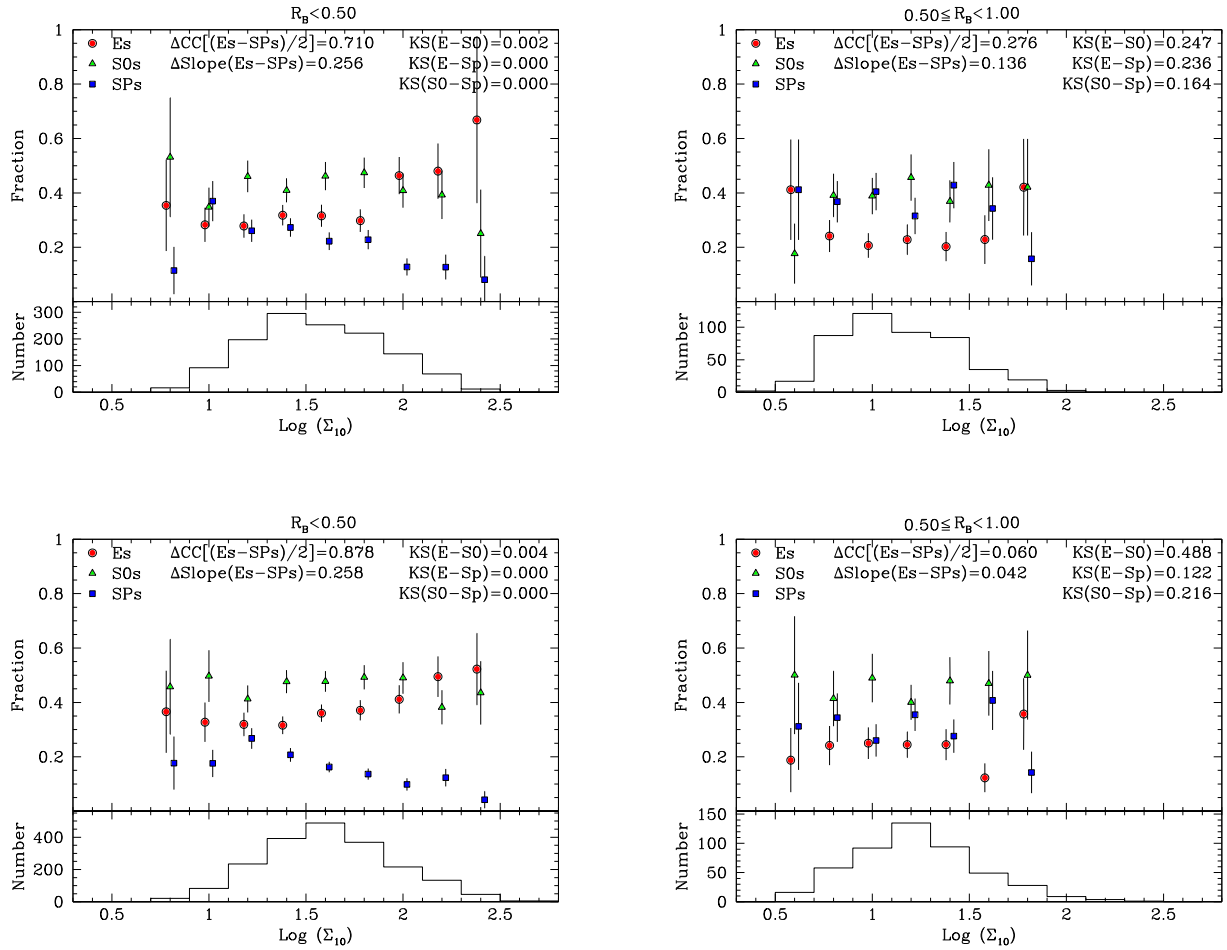

Figure 11. T–Σ relation for clusters with log L_X < 44.15 (upper panels) and log $L_X \geq 44.15$ (bottom panels) in different ranges of clustercentric distance: $R_B < 0.5$ (left-hand panels) and $0.5 \leq R_B < 1$ (right-hand panels). Again, the T–Σ relation appears to hold just in the inner cluster regions, irrespective of the cluster X-ray luminosity. The meaning of the symbols is as in Fig. 6.

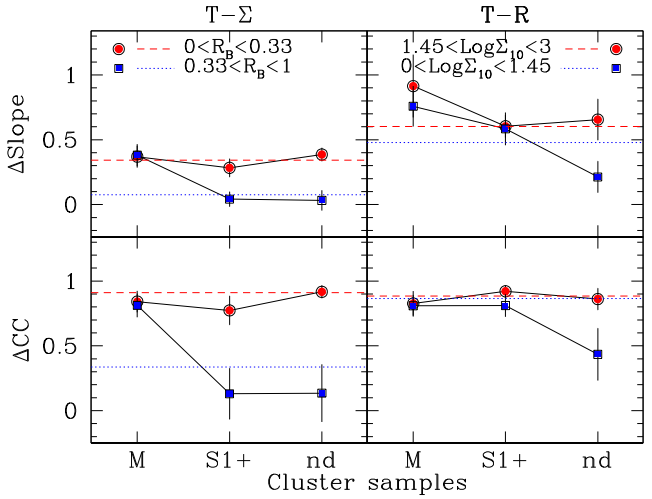

Figure 12. Coefficients ΔSlope (upper panels) and ΔCC (lower panels) of the T–Σ (left-hand panels) and T–R (right-hand panels) relations for the three cluster subsamples (M, $S1+$ and nd) defined in Section 6.3.2. The full dots and squares (red and blue in the electronic version) refer to different ranges of R_B and log Σ_{10}, for the T–Σ and T–R relations, respectively. The dashed and dotted lines (again red and blue in the electronic version) correspond to the values found in the different cases for the whole sample of WINGS clusters.

Fig. 14 illustrates the results. It clearly shows that, while for the T–R relation both ΔSlope and ΔCC turn out to be almost stable in the four bins of log (M_*), they are strongly increasing functions of the galaxy stellar mass for the T–Σ relation. In particular, in the lowest mass bin, both ΔSlope and ΔCC indicate that the T–Σ is almost absent.

We have also tried to account for spectroscopic incompleteness by applying a statistical correction to our sample. This is obtained by weighting each galaxy by the inverse of the ratio of the number of spectra yielding a redshift to the total number of galaxies in the photometric catalogue, in bins of 1 mag (Cava et al. 2009). We do not report here the results of such additional analysis. We just mention that they turn out to be quite similar to those shown in Table 4 and in Fig. 14.

This might induce to draw the conclusion that the lack of T–Σ we observe outside the inner cluster regions is due to an excess in these regions of galaxies in the lowest stellar mass bin with respect to the other bins. However, this conclusion turns out to be ruled out by the 2S-KS applied to the clustercentric distances of galaxies in the four mass bins.

It is well known (see e.g. Vulcani et al. 2011) that the three broad morphological types (E/S0/Sp) have quite different stellar mass distributions. This is confirmed by the 2S-KS applied to our galaxy sample. It might be speculated that this fact, combined with the dependence of the mass distribution on the local density

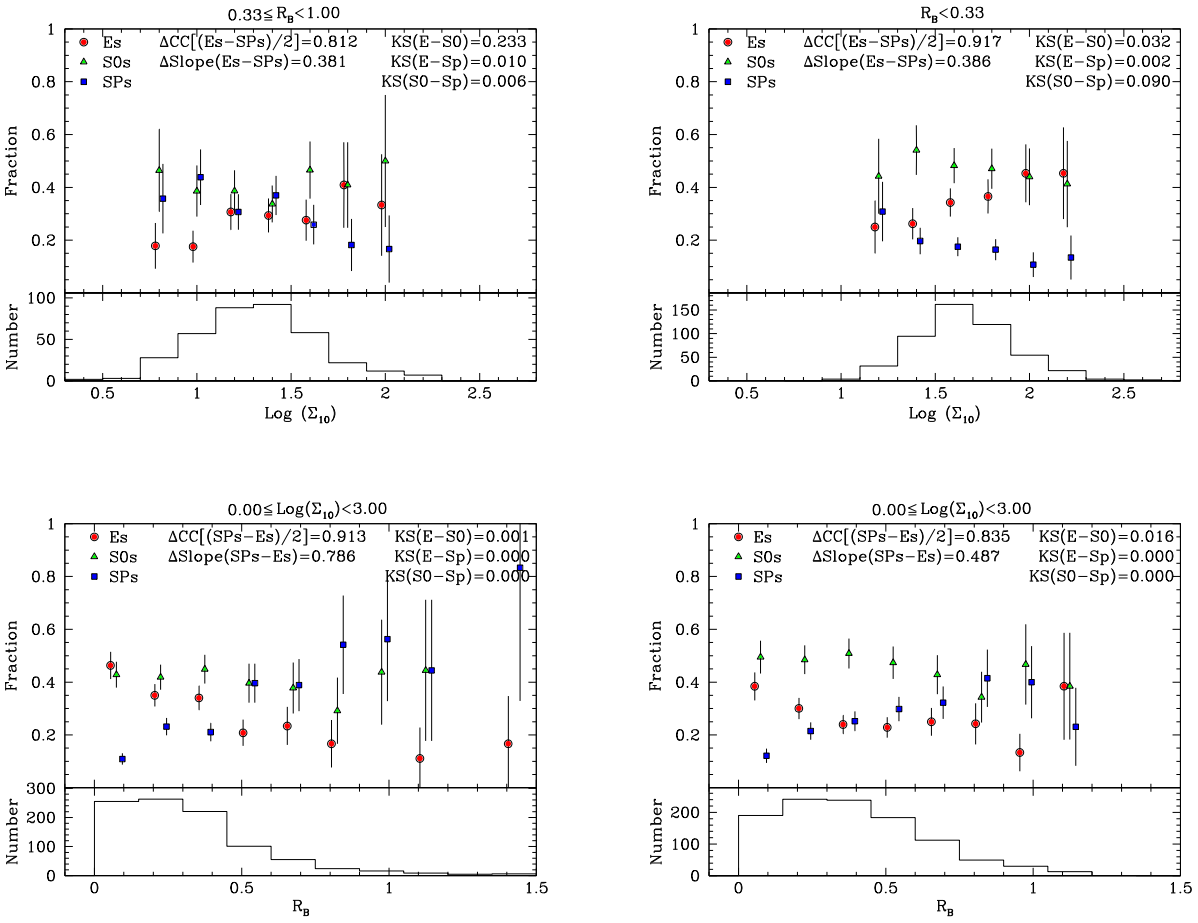

Figure 13. T–Σ and T–R relations (upper and bottom panels, respectively) for regular (left-hand panels; sample *M*) and very irregular (right-hand panels; sample *nd*) clusters. The R_B and Σ_{10} intervals tried out in each case are indicated on the top of each panel. The meaning of the symbols is as in Fig. 6.

Table 4. Similar to Table 1, but for two different intervals of log (M_*).

		T–Σ				T–R		
log (M_*)	R_B	ΔCC	ΔSlope	KS(E–Sp)	log Σ_{10}	ΔCC	ΔSlope	KS(E–Sp)
	All	0.508	0.195	0.001	0–3	0.697	0.510	0.000
	(716)	(0.185)	(0.096)		(716)	(0.149)	(0.149)	
<10.76	0–0.5	0.679	0.290	0.009	0–1.45	0.467	0.404	0.006
	(523)	(0.150)	(0.103)		(365)	(0.213)	(0.240)	
	0.5–1	−0.020	−0.057	0.168	1.45–3	0.638	0.554	0.002
	(182)	(0.337)	(0.327)		(351)	(0.197)	(0.210)	
	All	0.879	0.354	0.000	0–3	0.876	0.681	0.000
	(824)	(0.055)	(0.053)		(809)	(0.071)	(0.118)	
>10.76	0–0.5	0.738	0.280	0.004	0–1.45	0.753	0.644	0.001
	(590)	(0.120)	(0.081)		(395)	(0.134)	(0.207)	
	0.5–1	−0.183	−0.096	0.404	1.45–3	0.772	0.637	0.001
	(225)	(0.289)	(0.186)		(414)	(0.142)	(0.190)	

(Vulcani et al. 2012), is fully responsible of the very existence of the T–Σ relation. In other words, the T–Σ could just be a consequence of the combined dependence of both the morphology and the local density on the stellar mass. This hypothesis would obviously imply that the T–Σ relation should not be observed at any (fixed) galaxy mass.

The upper panel of Fig. 15 contradicts such an expectation. It shows that, in spite of the poor statistics (218 galaxies), the T–Σ turns out to be remarkably strong even in quite narrow stellar mass bins (11 < log (M_*) < 11.3). For the sake of clarity, in this plot we use the histograms to represent the T–Σ, instead of the points, since the big error bars associated with the points should weight down too much the figure. It is also worth noticing that we have chosen the narrow mass bin in the high-mass part of the mass distribution, since the T–Σ progressively weakens towards low-mass galaxies (see Fig. 14). The lower panel of Fig. 15 shows that, similarly to T–Σ, the T–R relation appears to be strong enough also in a narrow stellar mass bin, while, at variance with the T–Σ (and according to Fig. 14), it is quite strong also for galaxies in the low-mass region of the distribution (10.3 < log (M_*) < 10.6).

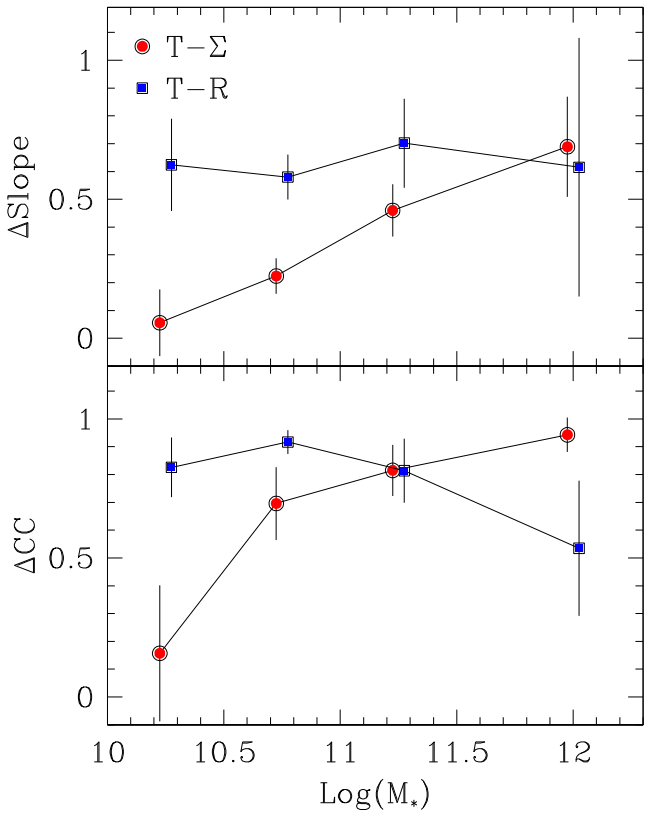

Figure 14. ΔSlope (upper panel) and ΔCC (lower panel) as a function of log (M_*) for both T–Σ (full dots; red in the electronic version) and T–R (full squares; blue in the electronic version).

7 SUMMARY AND OPEN ISSUES

In the present analysis, performed using the WINGS data base of galaxies in nearby clusters, we have shown that

(i) the correlation between morphological fractions and local density (T–Σ) exists only in the very inner regions of nearby clusters, almost vanishing outside $1/3\,R_{200}$, apart from very regular (non-substructured) clusters, for which the T–Σ relation also holds outside the inner regions;

(ii) in contrast, the strength of the correlation between morphological fractions and clustercentric distance (T–R) remains almost unchanged over the whole range of local density for both regular and irregular clusters, only slightly lessening for extremely clumpy clusters (bad centre determination?);

(iii) a couple of suitable tests and two different sets of numerical simulations support the validity of these results even considering the possible biases arising from the limited cluster area coverage of the WINGS imaging;

(iv) the above findings hold irrespective of both the global cluster mass (velocity dispersion and X-ray emission) and the stellar mass of galaxies;

(v) the strength of the T–Σ relation (where present) increases with increasing galaxy stellar mass, while this effect is not found for the T–R relation;

(vi) both the T–Σ (where present) and the T–R relations are remarkably strong even in quite narrow stellar mass bins. In particular, for the T–Σ relation, this rules out the hypothesis that it could just be a consequence of the combined dependence of both morphology and local density on stellar mass.

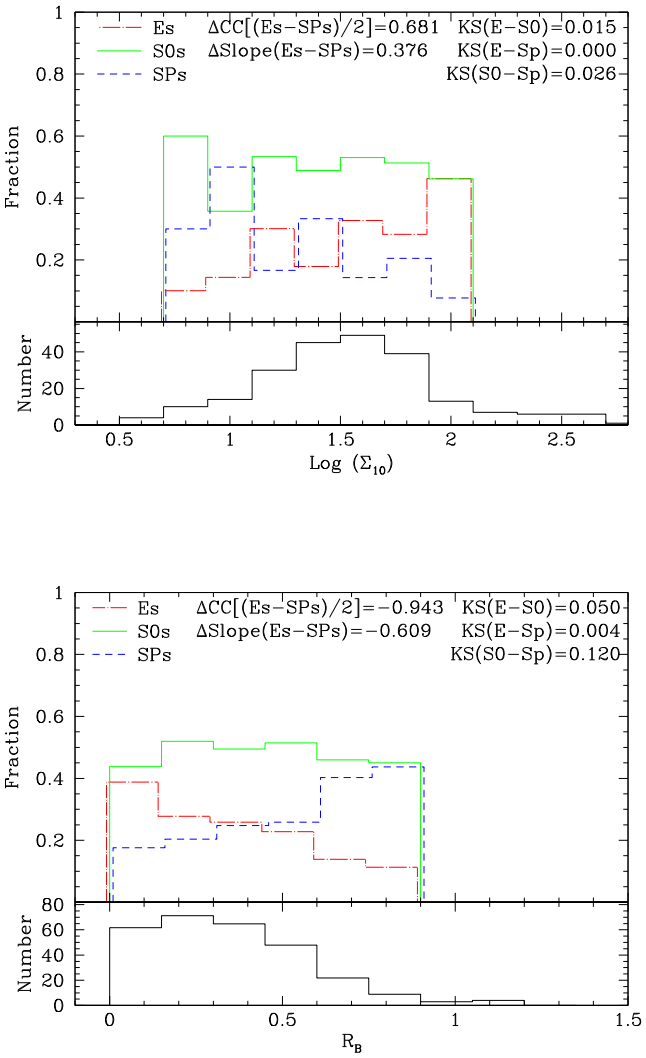

Figure 15. T–Σ (upper panel) and T–R (lower panel) for galaxies in the log (M_*) bins (11–11.3) and (10.3–10.6), respectively.

These results could lead us to conclude that the parameter actually driving morphological fractions in nearby clusters is the distance from the cluster centre, rather than the local density, as commonly believed. In this scenario the T–Σ relation would just be a by-product of the T–R relation, as already claimed by Whitmore & Gilmore (1993). Against this conclusion, however, one can bring forward the argument (challenged by Whitmore 1995) that the T–Σ relation is also found in the general field (groups+pairs+single galaxies; Bhavsar 1981; de Souza et al. 1982; Postman & Geller 1984; Helsdon & Ponman 2003). In fact, according to the standard paradigm, galaxy clusters are progressively built up through continuous infalling into the main cluster halo of galaxies coming from the surrounding field. Thus, it is worth asking oneself whether the lack of the T–Σ in the out-of-centre part of clusters really implies the fall of the T–Σ paradigm or, instead, some other mechanism should be invoked to interpret our findings.

First, we note that the results illustrated in this paper (Section 6.3.2, in particular) suggest that the T–Σ relation holds only in dynamically evolved regions of nearby clusters, i.e. the whole clusters, or just their inner parts, for regular ('relaxed') or substructured ('non-relaxed') clusters, respectively. Therefore, it seems to us that

the apt question is: what is causing the observed T–Σ weakening in dynamically 'non-relaxed' regions? We speculate that some mechanism of morphological broadening/redistribution is responsible for the T–Σ weakening in the intermediate regions of substructured ('non-relaxed') clusters.

Two different (and perhaps complementary) ways to attain this effect are conceivable: (i) general field galaxies lose (release) the dependence of their morphology on the local density when they infall into the cluster, recovering it only when (and where) the dynamical equilibrium has been already reached (only inner regions for substructured, 'non-relaxed' clusters); (ii) galaxies having already experienced the very dense interiors of clusters and moving back to the intermediate/outer regions, or 'free' galaxies coming in these regions from different subhaloes are 'T–Σ untied', thus diluting the relation likely existing in the infalling galaxy population.

The first mechanism could result from reshuffling of galaxy locations due the gravitational interactions within the cluster. The second mechanism envisages a scenario in which galaxies responsible for morphological broadening could come from the innermost cluster regions (likely after one or more passages close to the cluster centre) and/or could be detached from their original infalling haloes, therefore, losing their pristine correlation between morphology and Σ.

Of course, the two outlined mechanisms of morphological broadening could operate in tandem. Unfortunately, there are no observational hints about which one of them is prevailing, or even about their very existence. As a matter of fact, it is presently unknown which process is responsible for the weakening of T–Σ in the intermediate cluster regions. The increasingly powerful and sophisticated ΛCDM models of galaxy formation and evolution inside dark matter haloes could help shed some light on these findings.

ACKNOWLEDGEMENTS

We acknowledge partial financial support by contract PRIN/MIUR 2009: 'Dynamics and Stellar Populations of Superdense Galaxies' (Code: 2009L2J4MN) and by INAF/PRIN 2011: 'Galaxy Evolution with the VLT Survey Telescope (VST)'.

BV was supported by the World Premier International Research Center Initiative (WPI), MEXT, Japan, and by the Kakenhi Grant-in-Aid for Young Scientists (B)(26870140) from the Japan Society for the Promotion of Science (JSPS).

REFERENCES

Bamford S. P. et al., 2009, MNRAS, 393, 1324
Bell E. F., de Jong R. S., 2001, ApJ, 550, 212
Berta S. et al., 2006, A&A, 451, 881
Bhavsar S. P., 1981, ApJ, 246, L5
Bezanson R., Brammer G., Franx M., Labbé I., 2012, ApJ, 745, 179
Calvi R., Poggianti B. M., Vulcani B., 2011, MNRAS, 416, 727
Calvi R., Poggianti B. M., Fasano G., Vulcani B., 2012, MNRAS, 419, L14
Capak P., Abraham R. G., Ellis R. S., Mobasher B., Scoville N., Sheth K., Koekemoer A., 2007, ApJS, 172, 284
Cappellari M. et al., 2011, MNRAS, 416, 1680
Cava A. et al., 2009, A&A, 495, 707
Desai V. et al., 2007, ApJ, 660, 1151
de Souza R. E., Capelato H. V., Arakaki L., Logullo C., 1982, ApJ, 263, 557
de Vaucouleurs G., de Vaucouleurs A., Corwin H. G., Jr, Buta R. J., Paturel G., Fouqué P., 1991, Third Reference Catalogue of Bright Galaxies. Springer-Verlag, New York
D'Onofrio M. et al., 2014, A&A, 572, 87
Dressler A., 1980, ApJ, 236, 351 (D80)
Dressler A. et al., 1997, ApJ, 490, 577 (D97)
Driver S. P., Liske J., Cross N. J. G., De Propris R., Allen P. D., 2005, MNRAS, 360, 81
Ebeling H., Voges W., Bohringer H., Edge A. C., Huchra J. P., Briel U. G., 1996, MNRAS, 281, 799
Ebeling H., Edge A. C., Bohringer H., Allen S. W., Crawford C. S., Fabian A. C., Voges W., Huchra J. P., 1998, MNRAS, 301, 881
Ebeling H., Edge A. C., Allen S. W., Crawford C. S., Fabian A. C., Huchra J. P., 2000, MNRAS, 318, 333
Evrard A. E., Silk J., Szalay A. S., 1990, ApJ, 365, 13
Fasano G., Poggianti B. M., Couch W. J., Bettoni D., Kjærgaard P., Moles M., 2000, ApJ, 542, 673
Fasano G. et al., 2006, A&A, 445, 805 (F06)
Fasano G. et al., 2012, MNRAS, 420, 926 (F12)
Finn R. A. et al., 2005, ApJ, 630, 206
Fritz J. et al., 2007, A&A, 470, 137
Fritz J. et al., 2011, A&A, 526, 45
Fukugita M. et al., 2007, AJ, 134, 579
Goto T., Yamauchi C., Fujita Y., Okamura S., Sekiguchi M., Smail I., Bernardi M., Gomez P. L., 2003, MNRAS, 346, 601
Helsdon S. F., Ponman T. J., 2003, MNRAS, 339, L29
Holden B. P. et al., 2007, ApJ, 670, 190
Hubble E. P., Humason M. L., 1931, ApJ, 74, 43
Kroupa P., 2001, MNRAS, 322, 231
Lilly S. J. et al., 2007, ApJS, 172, 70
Lintott C. et al., 2011, MNRAS, 410, 166
Liske J., Lemon D. J., Driver S. P., Cross N. J. G., Couch W. J., 2003, MNRAS, 344, 370
Moretti A. et al., 2014, A&A, 564, A138
Morgan W. W., 1961, Proc. Natl. Acad. Sci. USA, 47, 905
Nuijten M. J., Simard L., Gwyn S., Röttgering H. J., 2005, ApJ, 626, L77
Oemler A., Jr, 1974, ApJ, 194, 1
Oesch P. A. et al., 2010, ApJ, 714, L47
Peacock J. A., 1999, Cosmological Physics. Cambrige Univ. Press, Cambridge
Peebles P. J. E., 1993, Principles of Physical Cosmology. Princeton Univ. Press, Princeton, NJ
Peng Y.-J. et al., 2010, ApJ, 721, 193
Pisani A., 1993, MNRAS, 265, 706
Pisani A., 1996, MNRAS, 278, 697
Poggianti B. M., 1997, A&AS, 122, 399
Poggianti B. M. et al., 2009, ApJ, 697, L137
Postman M., Geller M. J., 1984, ApJ, 281, 95
Postman M. et al., 2005, ApJ, 623, 721
Ramella M. et al., 2007, A&A, 470, 39
Schlegel D. J., Finkbeiner D. P., Davis M., 1998, ApJ, 500, 525
Scoville N. et al., 2007, ApJS, 172, 38
Smith G. P., Treu T., Ellis R. S., Moran S. M., Dressler A., 2005, ApJ, 620, 78
Spitzer L., Jr, Baade W., 1951, ApJ, 113, 413
Tasca L. A. M. et al., 2009, A&A, 503, 379
Thomas T., Katgert P., 2006, A&A, 446, 31
Treu T., Ellis R. S., Kneib J. P., Dressler A., Smail I., Czoske O., Oemler A., Natarajan P., 2003, ApJ, 591, 53
Valentinuzzi T. et al., 2009, A&A, 501, 851
van der Wel A., 2008, ApJ, 675, 13
van der Wel A. et al., 2007, ApJ, 670, 206
Varela J. et al., 2009, A&A, 497, 667
Vulcani B. et al., 2011, MNRAS, 413, 921
Vulcani B. et al., 2012, MNRAS, 420, 1481
Whitmore B. C., 1995, in Richter O.-G., Borne K., eds, ASP Conf. Ser. Vol. 70, Groups of Galaxies. Astron. Soc. Pac., San Francisco, p. 41
Whitmore B. C., Gilmore D. M., 1991, ApJ, 367, 64
Whitmore B. C., Gilmore D. M., 1993, ApJ, 407, 489
Wilman D. J., Oemler A., Jr, Mulchaey J. S., McGee S. L., Balogh M. L., Bower R. G., 2009, ApJ, 692, 298

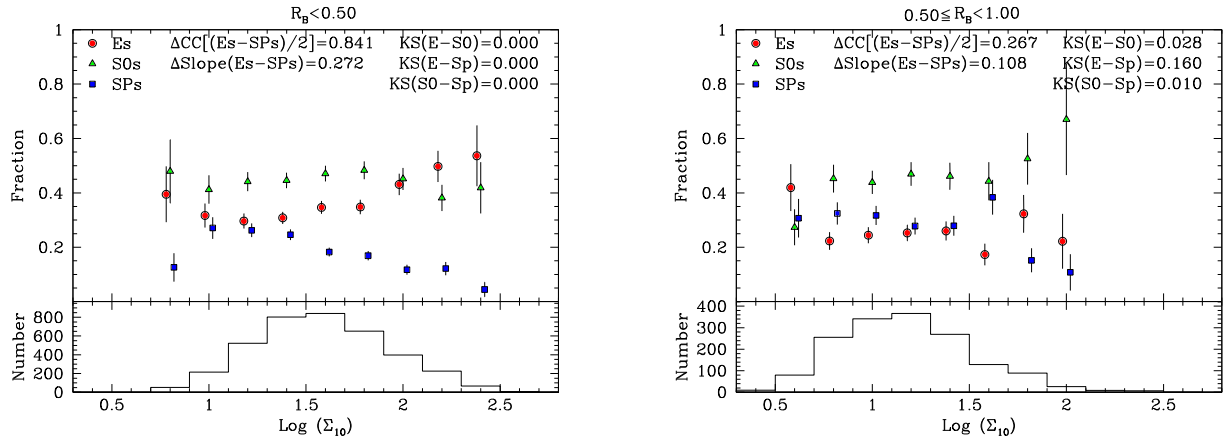

Figure A1. T–Σ for WINGS galaxies with $R_B < 0.5$ (in units of R_{200}; left-hand panel) and $0.5 \leq R_B < 1$ (right-hand panel). The galaxies have been weighted according to the inverse of their circumferential coverage (see text). The meaning of the symbols is as in Fig. 6.

APPENDIX A: TESTING THE EFFECTS OF THE LIMITED CLUSTER AREA COVERAGE

The following three tests have been devised with the aim of investigating the effects of the irregular and/or limited cluster coverage of the WINGS imaging on the results we present about the T–Σ relation in Section 6.1 and, marginally, about the T–R in Section 6.2.

A1 Irregular image shape

In the first test, using the same galaxy sample of Section 6, we produce a new versions of the T–Σ relation in which each galaxy, with its proper clustercentric distance (R_B), is weighted according to the inverse of its circumferential coverage, that is the fraction of circumference (of radius R_B) covered by the image. This is equivalent to assume that, for each galaxy falling into the image, other (similar) galaxies could exist at the same clustercentric distance, but falling outside the image. This weighting also (obviously) increases the 'nominal' number of galaxies (in particular spirals), part of them being actually virtual objects. This test tries to partially account for the non-circular (and irregular) shape of our images (from INT, in particular).

Fig. A1 is similar to Fig. 7, but it is obtained using the above outlined weighting procedure of galaxies. From the comparison between Figs 7 and A1 we conclude that the non-circular and irregular shape of the images should not invalidate the conclusion reported in Section 6.2 that the strength of the T–Σ relation in clusters strongly depends on the clustercentric distance.

A2 Limited cluster area coverage

In the second test, we compare the T–Σ obtained using galaxies in the whole cluster sample with the corresponding ones in which only galaxies in clusters with large values of the cluster area coverage are included. This is equivalent to bias the analysis towards smaller and more distant clusters.

Table A1 is similar to Table 1, but it reports the results for just the T–Σ and for two different values of the minimum allowed coverage fraction (CF > 0.5 and CF > 0.75). More precisely, to assume for instance CF > 0.5, means that just galaxies in clusters whose CF in the considered range of R_B is greater than 0.5 are each time included in the sample. This obviously reduces the number of employed galaxies, but makes the T–Σ relation more robust against the CF issue. From the comparison between Tables 1 and A1 we conclude again that the limited cluster area coverage of the images does not invalidate the conclusion reported in Section 6.2 that the strength of the T–Σ relation in clusters strongly depends on the clustercentric distance.

Table A1. Similar to Table 1, but for just T–Σ and for two different values of the minimum coverage fraction (CF).

		T–Σ		
CF	R_B	ΔCC	ΔSlope	KS(E–Sp)
	0–1	0.853	0.352	0.000
	(1710)	(0.065)	(0.057)	
CF = 0.5	0–0.5	0.878	0.282	0.000
	(3351)	(0.056)	(0.041)	
	0.5–1	−0.087	0.022	0.210
	(454)	(0.278)	(0.123)	
	0–1	0.782	0.512	0.000
	(381)	(0.106)	(0.137)	
CF = 0.75	0–0.5	0.885	0.286	0.000
	(2551)	(0.051)	(0.040)	
	0.5–1	−0.327	−0.138	0.037
	(127)	(0.290)	(0.394)	

A3 Numerical simulations

Finally, we use two different sets of numerical simulations to investigate the effect of the limited cluster area coverage on the T–Σ in different ranges of the clustercentric distance. In order to perform the simulations we have to assume some dependence of the morphological fractions on either R or Σ_{10} (or even on both). Therefore, these simulations can also be used, in principle, to test which one of the two (or three) hypotheses is able to reproduce the observed T–Σ and T–R relations.

The first set (Simulation Set 1: SS1) totally ignores the physics of the clusters. It simply produces artificial samples of points with random polar angles (circular symmetry) and radial coordinates randomly extracted from a distribution suitably chosen in order to reproduce the R_B–log Σ_{10} relation observed in the WINGS galaxy sample. Once the Σ_{10} values of the simulated points have been

Table A2. Simulation Set 1 (SS1). Since the simulations of this set turn out to be rather consuming in terms of CPU time, the number of throws used here to obtain the distributions of coefficients CCdev, P_{CC}, SLdev and P_{SL} varies from 100 to 200.

	T–Σ					*T*–*R*			
R_B interval	CCdev	P_{CC}	SLdev	P_{SL}	log Σ_{10} interval	CCdev	P_{CC}	SLdev	P_{SL}
HΣ_{10}									
0–1	1.13	0.32	0.10	0.90	0–3	1.10	0.14	**4.02**	**0.00****
0–0.5	1.50	0.24	0.61	0.49	0–1.45	1.42	0.08	1.90	0.07
0.5–1	**4.04**	**0.01***	1.85	**0.03**	1.45–3	1.11	0.12	1.82	**0.02**
H*R*									
0–1	0.11	0.86	1.79	**0.02**	0–3	1.18	0.22	0.04	0.92
0–0.5	0.83	0.23	**3.21**	**0.00****	0–1.45	0.12	0.92	0.87	0.34
0.5–1	0.00	0.99	0.50	0.65	1.45–3	0.17	0.82	0.07	0.94
HMIX									
0–1	0.10	0.96	0.93	0.26	0–3	0.29	0.66	1.56	0.10
0–0.5	0.14	0.93	0.99	0.33	0–1.45	0.70	0.32	0.47	0.57
0.5–1	1.44	0.31	0.61	0.60	1.45–3	0.69	0.36	1.29	0.25

Table A3. Simulation Set 2 (SS2). The simulations of this set are much faster than in the case of SS1. Therefore, the number of throws used here to obtain the distributions of coefficients CCdev, P_{CC}, SLdev and P_{SL} is everywhere 1000.

	T–Σ					*T*–*R*			
R_B interval	CCdev	P_{CC}	SLdev	P_{SL}	log Σ_{10} interval	CCdev	P_{CC}	SLdev	P_{SL}
HΣ_{10}									
0–1	1.11	0.33	0.19	0.86	0–3	1.14	0.18	**4.31**	**0.00****
0–0.5	1.47	0.24	0.51	0.61	0–1.45	1.33	0.07	**3.24**	**0.00****
0.5–1	**5.64**	**0.00****	2.16	**0.04**	1.45–3	1.21	0.11	**3.23**	**0.00****
H*R*									
0–1	0.28	0.76	2.29	**0.02**	0–3	1.72	0.12	0.05	0.94
0–0.5	0.66	0.44	2.72	**0.01***	0–1.45	1.72	0.18	1.53	0.14
0.5–1	0.03	0.97	0.51	0.61	1.45–3	0.98	0.41	0.13	0.92
HMIX									
0–1	0.30	0.77	1.25	0.18	0–3	0.00	0.99	2.21	**0.03**
0–0.5	0.21	0.82	1.19	0.26	0–1.45	0.34	0.73	0.84	0.41
0.5–1	1.76	0.18	0.74	0.44	1.45–3	0.48	0.61	1.59	0.10

computed in the usual way, the artificial sample is randomly thinned out following a depletion law depending on the radial coordinate and suitably chosen in order to reproduce the variation of the total number density of the WINGS sample as a function of R_B. This procedure should properly account for the incompleteness of the real sample due to both the irregular image shape and the limited coverage fraction. However, the lack of physics, in particular of gravitational clustering (two- or three-point correlation function), makes the scatter of Σ_{10} in the simulated *R*–log Σ_{10} relations lower than in the real sample of WINGS galaxies. We compensate this lack of physics through an additional scatter on Σ_{10}, tuned on the observed *R*–log Σ_{10} relation and depending on the radial coordinate. Then, we consider the two alternative hypothesis that the morphological fractions (F_E and F_S) depend either just on Σ_{10} (Hypothesis Σ_{10}: HΣ_{10}) or just on *R* (H*R*). We assume in the two cases the probability that the points in our simulated samples were elliptical or spiral galaxies to coincide with the weighted linear fits of the relations in Fig. 6 [$F_E(\Sigma_{10})$ and $F_S(\Sigma_{10})$] or in Fig. 8 [$F_E(R_B)$ and $F_S(R_B)$], respectively. They are

$$F_E = 0.125 + 0.136 \log \Sigma_{10}; \quad F_S = 0.493 - 0.177 \log \Sigma_{10},$$

$$F_E = 0.401 - 0.25\, R_B; \quad F_S = 0.091 + 0.368\, R_B.$$

We also formally contemplate the 'mixed' hypothesis (HMIX), in which the morphological fractions depend on both Σ_{10} and *R*. In this case we roughly assume

$$F_E = [F_E(\Sigma_{10}) + F_E(R)]/2; \quad F_S = [F_S(\Sigma_{10}) + F_S(R)]/2.$$

In the second set of simulations (SS2) we adopt the same procedure to randomly assign the morphological type, but we use the real sample of WINGS galaxies to take the (measured) values of Σ_{10} and *R*.

For both kinds of simulations (SS1 and SS2) and for each hypothesis about the dependence of the morphological fractions (HΣ_{10}, H*R*, HMIX), we make several throws, each throw producing *T*–Σ and *T*–*R* relations similar to those illustrated in Figs 6–9 (*R* intervals: 0–1, 0–0.5, 0.5–1; log Σ_{10} intervals: 0–3, 0–1.45, 1.45–3), with the same number of points (galaxies). Moreover, for each throw we record the values of the coefficients ΔCC and ΔSlope defined in Section 6.1. Finally, in each case, we compare the distributions of ΔCC and ΔSlope with the corresponding values obtained for the real sample of WINGS galaxies (see the previously mentioned figures). In this way, for both SS1 and SS2, we can associate with each hypothesis (HΣ_{10}, H*R*, HMIX) and for both the *T*–Σ and *T*–*R* relations (in the corresponding intervals of *R* and Σ_{10}, respectively) a set of deviates of the observed coefficients ΔCC and ΔSlope (CCdev and SLdev; both in rms units) with respect to the

corresponding distributions, as well as a set of probabilities (P_{CC} and P_{SL}) that these coefficients are extracted from the distributions themselves.

Tables A2 and A3 illustrate the results obtained for the two sets of simulations (SS1 and SS2, respectively). For each hypothesis (HΣ_{10}, HR, HMIX), the tables report the deviates and the probabilities of the coefficients ΔCC and ΔSlope of the observed T–Σ and T–R relations for different intervals of R and log Σ_{10}, respectively. They are computed comparing each coefficient with the corresponding, proper distribution obtained from the simulations. It should be noted that, due to the rather cumbersome (and CPU time consuming) procedure needed to produce a single SS1 sample, the number of throws used to obtain the distributions of coefficients CCdev, P_{CC}, SLdev and P_{SL} is almost one order of magnitude smaller for SS1 (N_{sim} = 100/200) than for SS2 (N_{sim} = 1000). This fact, together with the use of the real WINGS quantities (Σ_{10} and R_B) in SS2, suggests that the robustness of the results is greater for SS2 than for SS1. In both Tables A2 and A3 we report in boldface those values of CCdev and SLdev larger than 3, as well as those values of P_{CC} and P_{SL} lower than 0.05. Moreover, we mark with one or two asterisks those values of P_{CC} and P_{SL} equal to or less than 0.01, respectively.

In spite of the quite rough procedure used to generate the simulated samples in the SS1 and to attribute the morphological type to each simulated point (in both SS1 and SS2), Tables A2 and A3 provide us with some indication about the driving parameter of the morphological fractions in clusters.

(i) The 'canonical' hypothesis that the morphological fractions in clusters just depend on the local density (HΣ_{10}) is not able to reproduce the observed T–R relation, either for the whole sample or for the two Σ_{10} intervals. This is particularly evident in Table A3.

(ii) Although specifically built to obey the observed morphology–density relation, the HΣ_{10} simulations just marginally reproduce the very T–Σ relation in the outer part of clusters (R interval: 0.5–1), usually producing much steeper and more correlated distributions than the observed one (see light histograms in Fig. A2). While for SS1 this might be thought as a consequence of the quite regular shape of the simulated clusters (see Section 6.3.2), such an explanation is ruled out by SS2, where the observed WINGS quantities (Σ_{10} and R_B) have been used.

(iii) On the contrary, the alternative hypothesis that the morphological fractions in clusters just depend on the clustercentric distance (HR) quite well reproduces both the T–R relation (in any Σ_{10} interval) and the T–Σ relations in the outer cluster regions (see dark histograms in Fig. A2), but it seems to fail in reproducing the T–Σ in the inner cluster regions. This is particularly true for the SS1 (Table A2).

(iv) The mixed hypothesis that the morphological fractions actually depend on both Σ_{10} and R (HMIX) turns out to be fairly consistent with all observed T–Σ and T–R relations, but (perhaps) the T–R in the full log Σ_{10} interval (0–3).

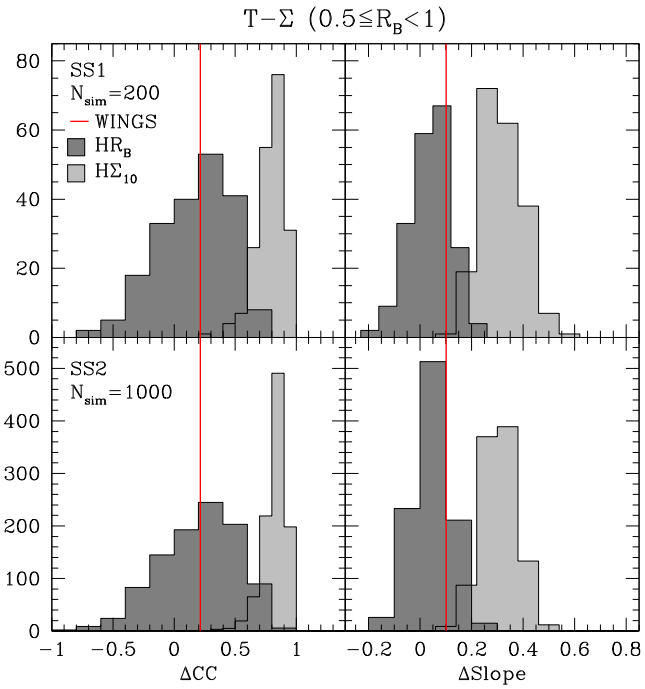

Figure A2. Results of the simulations SS1 (upper panels) and SS2 (lower panels) for the T–Σ in the R interval (0.5–1). The left- and right-hand panels illustrate the distributions of ΔCC and ΔSlope, respectively. The dark and light histograms refer to the HR and HΣ_{10} hypotheses, respectively.

The above remarks seem to favour the HR hypothesis with respect to the classical HΣ_{10} scenario, although this result might critically depend on the simulation procedure and might be modified, for instance, by a different (not linear) representation of the relations $F_E(\Sigma_{10})$, $F_S(\Sigma_{10})$, $F_E(R)$ and $F_S(R)$.

SUPPORTING INFORMATION

Additional Supporting Information may be found in the online version of this article:

(http://mnras.oxfordjournals.org/lookup/suppl/doi:10.1093/mnras/stv500/-/DC1).

Please note: Oxford University Press is not responsible for the content or functionality of any supporting materials supplied by the authors. Any queries (other than missing material) should be directed to the corresponding author for the article.

This paper has been typeset from a TEX/LATEX file prepared by the author.